Lawrence Berkeley National Laboratory
Recent Work

Title
NUCLEAR QUADRIPOLE INTERACTION STUDIES BY PERTURBED ANGULAR CORRELATIONS

Permalink
https://escholarship.org/uc/item/6nh7w8km

Authors
Haas, H.
Shirley, D.A.

Publication Date
1972-10-01

eScholarship.org Powered by the California Digital Library
University of California

Submitted to Journal of
Chemical Physics

RECEIVED
LAWRENCE
RADIATION LABORATORY

JAN 12 1973

LIBRARY AND
DOCUMENTS SECTION

LBL-1284
Preprint

NUCLEAR QUADRUPOLE INTERACTION STUDIES BY PERTURBED ANGULAR CORRELATIONS

H. Haas and D. A. Shirley

October 1972

Prepared for the U.S. Atomic Energy
Commission under Contract W-7405-ENG-48

For Reference

Not to be taken from this room

LBL-1284

DISCLAIMER

This document was prepared as an account of work sponsored by the United States Government. While this document is believed to contain correct information, neither the United States Government nor any agency thereof, nor the Regents of the University of California, nor any of their employees, makes any warranty, express or implied, or assumes any legal responsibility for the accuracy, completeness, or usefulness of any information, apparatus, product, or process disclosed, or represents that its use would not infringe privately owned rights. Reference herein to any specific commercial product, process, or service by its trade name, trademark, manufacturer, or otherwise, does not necessarily constitute or imply its endorsement, recommendation, or favoring by the United States Government or any agency thereof, or the Regents of the University of California. The views and opinions of authors expressed herein do not necessarily state or reflect those of the United States Government or any agency thereof or the Regents of the University of California.

NUCLEAR QUADRUPOLE INTERACTION STUDIES BY PERTURBED ANGULAR CORRELATIONS*

H. Haas and D. A. Shirley

Department of Chemistry and
Lawrence Berkeley Laboratory
University of California
Berkeley, California 94720

October 1972

ABSTRACT

A comprehensive study was made of the applicability of gamma-ray angular correlations to the determination of quadrupole interactions in metals and insulating solids. Dynamic effects were studied in solutions and gases. A total of fourteen gamma-ray cascades were employed. Several nuclear spins were confirmed, and the quadrupole moments of ten excited nuclear states were determined or estimated from the data. Quadrupole coupling constants were determined for excited states of the following nuclei in metallic host lattices of the same element: ^{44}Sc, ^{99}Ru, ^{111}Cd, ^{117}In, ^{187}Re, ^{199}Hg. Coupling constants were also measured for the following isotope (lattice) combinations: ^{99}Ru(Zn, Cd, Sn, Sb), ^{100}Rh(Zn, Ru, Cu_5Zn_8, Pd_2Al, $PdPb_2$), ^{111}Cd(In, Hg, Tl, CdSb, Cd_3Ag, Zn, Ga, In, Sn, Sb, Bi, AuIn, InBi, In_2Bi), ^{115}In(Cd), ^{117}In(Cd, Sn), ^{131}I(Te), ^{181}Ta(HfB_2, $HfSi_2$), ^{204}Pb(Cd, In, Sn, As, Sb, Bi, Hg, Tl, $PdPb_2$).

Systematic variations of e^2qQ with host-lattice structure was observed, and host and solute properties were found to be separable to some extent for non-transition metals.

The nuclei ^{111}Cd, ^{115}In, ^{117}In, ^{199}Hg, and ^{204}Pb were used to determine a total of fifty quadrupole coupling constants in insulators, including twenty with nonzero asymmetry parameters, which give oscillatory but aperiodic correlation functions. It was strikingly (and exhaustively) demonstrated that good determinations of quadrupole coupling constants could be made following isomeric transitions (with no elemental transmutation) and beta decay (<u>with</u> elemental transmutation). However, in no case was it possible to derive a coupling constant from a gamma-ray cascade preceded directly by electron-capture decay, presumably because the sudden creation of a K-hole and the Auger and "shake-off" events that follow destroy the chemical integrity of the species under study.

Relaxation times were determined for a number of liquid samples. Studies of dimethyl-^{111m}Cd in various buffer gases showed that the spin memory was lost in one collision with heavy molecules, but that light molecules required several collisions.

0 0 0 0 3 6 0 0 0 4 1

NUCLEAR QUADRUPOLE INTERACTION STUDIES BY PERTURBED ANGULAR CORRELATIONS

H. Haas and D. A. Shirley

OUTLINE

0 0 0 0 3 6 0 0 0 4 2

I. INTRODUCTION

The first measurements of perturbed γ-γ angular correlation (PAC) were done in the early 1950's.[1] Many PAC studies of the interaction between magnetic fields and nuclear magnetic moments have subsequently been reported, but interest in the interaction between electric field gradients and nuclear quadrupole moments has increased only recently. If one compares the two measurements on the same nuclear state, a quadrupole interaction study is more complicated than a magnetic investigation for a number of reasons:

a) Electric field gradients of sufficient magnitude cannot be produced externally and thus cannot be varied at will.

b) Field gradients in most solids cannot be calculated with high accuracy.

c) The sign of the interaction is not obtained by a simple PAC experiment.

d) The effect observed is generally smaller, due to the presence of several frequencies.

e) Proper sample preparation is more important, as crystalline sources of appropriate structure have to be used.

Nevertheless, a PAC measurement of the nuclear quadrupole interaction with modern electronic equipment may in many cases be considered a simple experiment. This also holds for investigations of the fluctuating field gradients in liquids or gases. The present study was therefore made to obtain a clearer picture of the possibilities and limitations of the PAC technique as applied to nuclear quadrupole interactions.

The theory required for this work is described in Sec. II. Decay schemes are summarized in Sec. III. Section IV describes experimental procedures, and Sec. V gives nuclear properties. The results, given in Sec. VI, are classified according to the nature of the sample, with metals, insulators, liquids, and gases being treated in that order. The effect of the preceding decay mode is considered in the subsection on insulators. General conclusions are briefly stated in Sec. VII.

II. THEORY

The probability for observation of the 2γ quanta in direction $\vec{k}_1$ at time 0 and $\vec{k}_2$ at time t is described by the trace of the density matrix for emission of γ_1 and γ_2:

$$W(\vec{k}_1,\vec{k}_2,t) = \mathrm{Tr}[\rho(\vec{k}_1,0)\rho(\vec{k}_2,t)] \quad . \tag{1}$$

The density matrices are related to the angular correlation coefficients by

$$\rho(\vec{k},0)_{m,m'} = \sqrt{4\pi} \sum_{\lambda} (-1)^m A_\lambda \begin{pmatrix} I & I & \lambda \\ m' & -m & \mu \end{pmatrix} Y_\lambda^\mu(\vec{k}) \quad , \tag{2}$$

(with $\mu = m - m'$). The time-evolution of the density matrix $\rho(\vec{k},0)$ is governed by the von Neumann equation

$$\dot{\rho} = -\frac{i}{\hbar}[H,\rho] \quad . \tag{3}$$

The well-known solution for a time-independent interaction Hamiltonian H is

$$\rho(t) = e^{-(i/\hbar)Ht}\, \rho(0)\, e^{(i/\hbar)Ht} \quad . \tag{4}$$

If the interaction is time-dependent, an analytic solution may be obtained only in special cases.

A. Static Perturbation Functions

1. Fixed Orientation

The angular correlation (1) may in general be expanded in spherical harmonics, where, for γ rays, under parity conservation, only even multipoles will contribute:

$$W(\vec{k}_1,\vec{k}_2,t) = \sum_{\lambda_1\mu_1} \sum_{\lambda_2\mu_2} A_{\lambda_1}(1)\, A_{\lambda_2}(2)[(2\lambda_2 + 1)]^{-1/2}\, G_{\lambda_1\lambda_2}^{\mu_1\mu_2}(t)\, Y_{\lambda_1}^{\mu^*}(\vec{k}_1)\, Y_{\lambda_2}^{\mu_2}(\vec{k}_2) \quad . \quad (5)$$

Only the perturbation factor $G_{\lambda_1\lambda_2}^{\mu_1\mu_2}(t)$ is influenced by the environment. For a unique interaction Hamiltonian the $2I + 1$ eigenvectors $\langle n_i|$ and eigenvalues E_{n_1} may be calculated and the perturbation factor obtained as

$$G_{\lambda_1\lambda_2}^{\mu_1\mu_2}(t) = \sum_{m_1m_2} \sum_{n_1n_2} (-1)^{2I + m_1 + m_2} [(2\lambda_1 + 1)(2\lambda_2 + 1)]^{1/2}\, e^{-(i/\hbar)(E_{n_1} - E_{n_2})t}$$

$$\times \begin{pmatrix} I & I & \lambda \\ m_1' & -m_1 & \mu_1 \end{pmatrix} \begin{pmatrix} I & I & \lambda_2 \\ m_2' & -m_2 & \mu_2 \end{pmatrix} \langle n_1|m_2\rangle^*\langle n_1|m_1\rangle\langle n_2|m_2'\rangle\langle n_2|m_1'\rangle^* \quad . \quad (6)$$

The perturbations expected for single-crystalline or oligo-crystalline material are easily calculated from this relation.

2. Random Orientation

For a sample without preferential orientation, the angular correlation only depends on the angle θ between $\vec{k}_1$ and $\vec{k}_2$ through

$$W(\theta,t) = \sum_{\lambda} A_{\lambda}(1)\, A_{\lambda}(2)\, G_{\lambda}(t)\, P_{\lambda}(\cos\theta) \quad . \tag{7}$$

For a unique, but randomly oriented static interaction, the integration over all possible orientations may be done explicitly. The perturbation function for this case is

$$G_{\lambda}(t) = \sum_{\mu} \sum_{m_1 m_2} \sum_{n_1 n_2} (-1)^{2I + m_1 + m_2} e^{-(i/\hbar)(E_{n_1} - E_{n_2})t} \begin{pmatrix} I & I & \lambda \\ m_1' & -m_1 & \mu \end{pmatrix} \begin{pmatrix} I & I & \lambda \\ m_2' & -m_2 & \mu \end{pmatrix}$$

$$\langle n_1|m_2\rangle^* \langle n_1|m_1\rangle \langle n_2|m_2'\rangle \langle n_2|m_1'\rangle^* \quad . \tag{8}$$

For cases in which there is a partial orientation or with time-independent, randomly oriented contributions to the interaction Hamiltonian, the integration over all orientations in Eq. 6 may be done numerically. In many practical cases the contribution of the $\lambda = 2$ term dominates; therefore

$$W(\theta,t) = 1 + A_{22}\, G_2(t)\, \left(\tfrac{3}{2}\cos^2\theta - \tfrac{1}{2}\right) \quad , \tag{9}$$

is a good approximation for the observed angular correlation. For the nuclear quadrupole interaction the Hamiltonian may be represented in the major axis system of the field gradient tensor as

$$H = \frac{e^2 Qq}{4I(2I-1)} \left[3I_z^2 - I(I+1) + \frac{\eta}{2}\left(I_+^2 + I_-^2\right)\right] \quad . \tag{10}$$

It is convenient to define an interaction frequency

$$\omega_q = \frac{e^2 Q q}{\hbar\, 4I(2I-1)} \quad , \tag{10'}$$

because for axially symmetric field gradients, with $\eta = \frac{q_{xx} - q_{yy}}{q_{zz}} = 0$, the observed perturbation function is periodic. That is, in the general expression

$$G_\lambda(t) = \sum_{n_1 n_2} C_\lambda(n_1,n_2) \cos(f(n_1,n_2)\omega_q t) \quad , \tag{11}$$

the factors f are simple integers. In general this does not hold for $\eta \neq 0$, and a numerical solution of the secular equation must then be made to obtain the eigenvectors $\langle n_i |$ of the Hamiltonian (Eq. 10). For practical applications of Eq. 11, two modifications are sometimes necessary. The limited resolving time of the experimental set-up might lead to a damping of the high frequency components in Eq. 11. The simplest way to take this into account is to introduce a time resolution function of the form $e^{-1/2(t/t_R)^2}$ in the coefficients C. Thus:

$$C'(n_1,n_2) = C(n_1,n_2)\, e^{-(1/2)(f(n_1,n_2)\omega_q t_R)^2} \quad . \tag{11'}$$

Similarly, if the interaction frequency is not unique, but shows a spread $\delta\omega$ one obtains, for a normal distribution $e^{-(1/2)[(\omega - \omega_0)/\delta\omega]^2}$ also a modification

of the coefficients C:

$$C''(n_1,n_2) = C(n_1,n_2)\, e^{-(1/2)(f(n_1,n_2)\delta\omega\, t)^2} \quad . \qquad (11'')$$

B. Time-Dependent Interactions

If the Hamiltonian operating on the system is time-dependent, the solution of the differential equation (3) cannot in general be written down in closed form. However, theories for a number of special cases have been developed. All of them require stationary fluctuations of the Hamiltonian, which limits their usefulness. Time-dependent effects of the nuclear decay preceding the observed cascade ("after-effects") are not of this type, for example.

The simplest case is that of a short correlation time, $\tau_c << \frac{1}{\omega_q}$. That is, the density matrix elements change little between changes of the interaction Hamiltonian. This case was treated by Abragam and Pound (2) as early as 1953. They obtained:

$$G_\lambda(t) = e^{-k_\lambda t} \quad , \qquad (12)$$

with

$$k_\lambda = \frac{3}{5}\overline{\omega_q^2}\,\tau_c\lambda(\lambda+1)[4I(I+1) - \lambda(\lambda+1) - 1] \quad . \qquad (12')$$

The theory has been generalized recently to include the presence of static interactions (3). While the simple exponential behavior predicted by Eq. 12 may be easily verified experimentally, evidence for the multiexponential decay predicted by a more general treatment is still not unambiguous (4). The limit of long correlation time $\tau_c >> \frac{1}{\omega_q}$ may also be treated explicitly (5).

Recently some special cases have been solved for arbitrary correlation time (6,7). Experiments with simple systems, as close as possible to the theoretical models, would therefore be of great value. The same holds for the effects predicted for anisotropic molecular motion (8). Using a Monte Carlo program (for $I = 1, \frac{5}{2}$) on the basis of Eq. 3, it has been possible to reproduce the theoretical calculations with sufficient accuracy to warrant a treatment of the more complicated situation encountered in most experiments.

0 0 0 0 3 8 0 0 0 4 5

III. DECAY SCHEMES

For a PAC experiment a radioactive source that decays through a γ-γ cascade is required. The simple decay scheme in Fig. 1 shows all the features to be considered. If the source is not produced continuously, its halflife should be at least 15 minutes. The type of decay preceding the γ-γ cascade determines the kind of information obtainable. Because of detection problems, experiments with γ-ray energies below 10 keV are difficult. High conversion coefficients $[(1 + \alpha_1)(1 + \alpha_2) > 100]$ tend to reduce coincidence counting rates below a tolerable level. Similarly a branching ratio to the cascade of at least 0.1% of the total decay is necessary. Direct feeding of the intermediate state from the parent is especially troublesome. Because of time-resolution limits, the intermediate-state halflife should be at least 1 nsec. The random coincidences place a practical upper limit of about 10 μsec on this halflife. The unperturbed anisotropy for a PAC experiment should be at least 0.02, both to facilitate obtaining the necessary statistical accuracy and to compensate for possible systematic errors of this order of magnitude. Statistical accuracy for cascades involving short-lived states is limited by the counting rates that the detector can tolerate, while for long-lived states the chance

coincidence rate is the limiting factor. The relevant properties of the cascades studied in this work are summarized in Table 1.

Table I. Relevant decay characteristics of sources used in this work

Isotope	Intermediate-state energy (keV)	I^{π}	$T_{1/2}$(nsec)	Parent	Parent Halflife and Decay Mode	$E(\gamma_1)$ (keV)	(%)	$\alpha_1^{(a)}$	$E(\gamma_2)$ (keV)	(%)	$\alpha_2^{(a)}$	A_2^{eff}
^{44}Sc	68	1^+	153	^{44}Ti	48y EC	78	100	0.02	68	100	0.1	+0.03
^{99}Ru	90	$3/2^+$	21	^{99}Rh	16d EC	354	20	0.01	90	80	0.1	-0.18
^{100}Rh	75	2^+	214.5	^{100}Pd	4d EC	84	70	0.4	75	70	0.5	+0.16
^{111}Cd	247	$5/2^+$	84	^{111}Ag	7.5d β^-	95	0.2	0.5	247	1	0.05	-0.13
^{111}Cd	247	$5/2^+$	84	^{111m}Cd	49m IT	150	100	1.5	247	100	0.05	+0.16
^{111}Cd	247	$5/2^+$	84	^{111}In	2.8d EC	173	100	0.1	247	100	0.05	-0.15
^{115}In	829	$3/2^+$	5.5	^{115}Cd	53h β^-	35	0.5	3.4	490	10	0.05	+0.08
^{117}In	659	$3/2^+$	60	^{117}Cd	2.4h β^-	89	7	1.0	345	16	0.01	-0.19
^{131}I	1727	$11/2^-$	5.9	^{131m}Te	30h β^-	102	5	0.8	200	10	0.03	+0.09
^{181}Ta	482	$5/2^+$	10.6	^{181}Hf	42d β^-	133	93	0.5	482	85	0.03	-0.20
^{187}Re	206	$9/2^-$	570	^{187}W	24h β^-	480	30	0.02	72	15	2.0	-0.07
^{199}Hg	158	$5/2^-$	2.3	^{199m}Hg	43m IT	375	100	3.0	158	100	0.3	+0.22
^{204}Pb	1274	4^+	260	^{204m}Pb	67m IT	912	98	0.06	375	99	0.04	+0.18
^{204}Pb	1274	4^+	260	^{204}Bi	11h EC	984	20	0.01	375	90	0.04	-0.05

[a]The conversion coefficient α is defined as the ratio of the conversion-electron intensity to the photon intensity.

IV. EXPERIMENTAL

A. Apparatus

Perturbed angular correlations may be studied with the classical 2-detector setup, using variable angle between the photon propagation directions $\vec{k}_1$ and $\vec{k}_2$. It is difficult and time-consuming to measure angular correlations quantitatively in this way, however, and large corrections are often employed. To overcome some of these difficulties, 3 detectors are sometimes used, with two γ_2 or "stop" detectors at fixed angles (e.g. 90° and 180°) relative to the γ_1, or start, detector. This technique partially eliminates corrections necessitated by background and the lifetime of the intermediate state, if the ratio $\frac{W(180)}{W(90)}$ is formed, but the reliability of the result suffers from the unequal efficiencies of the stop detectors. A four-detector system, as illustrated in Fig. 2a, can eliminate this drawback. By using two start detectors (A and B) and two stop detectors (C and D), four coincidences (AC, AD, BC, BD) can be registered, and by forming the ratio

$$A_2(t) = \frac{2}{3}\left(\sqrt{\frac{(AC)\ (BD)}{(AD)\ (BC)}} - 1\right) = \frac{2}{3}\left(\frac{W(180)}{W(90)} - 1\right) \approx A_{22}\ G_{22}(t) \quad ,$$

the detector efficiencies can be made to cancel. Naturally there is also an increase in the coincidence counting rate. This arrangement also eliminates

0 0 0 0 3 8 0 0 0 4 7

geometrical effects, so that no special care need be taken to center the sample. To avoid systematic errors from absorption of γ rays in the sample, however, flat sources had to be used in a number of cases reported below.

Time-differential observation of PAC can be improved by the use of a fast-slow coincidence system, with the fast circuit carrying the timing information and the slow circuit the energy information from the detector pulses. The coincidence system used in this work was of the fast-slow type, with an active delay line. The circuit was very straightforward and used conventional electronics. To assure that the "time-zero" channels of the four coincidences would coincide in the four quarters of the multi-channel analyzer, variable delays were used for the fast signals. The slow coincidence unit was the only part of the system not commercially available. Figure 2b shows schematically how the slow signals were processed to make use of as much timing information as possible. For investigations of intermediate states with halflives longer than $\sim$ 500 nsec, a system with separate fast-slow circuits for all detectors and passive delay lines could be used to reduce the background from random events, because energy gating on the fast signal would be done before the time-to-amplitude converter. Differential delay discriminators were used in this work to partially achieve the same effect.

The fast circuit and slow coincidence unit were adjusted with a source of prompt coincident photons, usually annihilation quanta from ^{22}Na. The time resolution of the whole setup was checked with the same source. In practically all cases NaI detectors were found to be most suited for detection of the γ-rays. A few cases required the improved time resolution afforded by tin-doped plastic scintillators. The higher energy resolution of semiconductor detectors was not found necessary. It was, however, quite important to adapt the thickness of the NaI crystals (1mm to 3") to the γ-ray energy, both to improve the time resolution and to reduce background from high energy γ rays. To reduce the contribution of low energy γ rays a set of absorbers was used for most experiments.

B. Sample Preparation

Most of the radioactive samples used in this study were produced in the Berkeley 88" Cyclotron or the Triga reactor of UC Berkeley. Separated isotope targets were obtained from Oak Ridge. The production of each radioisotope is described below, followed by a short description of the preparation of each source that was made from it.

^{44}Ti.

A 1.5 mm Sc metal disc was irradiated with 30 microampere hours (μAh) of 22 MeV protons. A cooling period of four weeks was allowed to eliminate ^{44m}Sc.

Sc: The sample was annealed 12 hrs at 1000°C in vacuum.

^{99}Rh.

Metallic ^{99}Ru was irradiated with 12-MeV protons, producing ^{99}Rh via a (p,n) reaction. Carrier-free ^{99}Rh was separated chemically as described earlier (9).

Ru: The target material was annealed at 1400°C in vacuum. Zn, Cd, Sn, Sb: The activity was electroplated onto Zn (Cd, Sn, Sb) foils which were then melted under H_2.

^{100}Pd.

This activity was made in two ways: a) Metallic ^{103}Rh was irradiated with 40 MeV protons, producing ^{100}Pd via a (p,4n) reaction. The ^{100}Pd was

separated chemically as described before (10). b) Metallic ^{99}Ru was irradiated with 35 MeV α's, producing ^{100}Pd by the (α,3n) reaction. Ru: The ^{99}Ru target material was annealed at 1400°C in vacuum. Zn: The ^{100}Pd activity was electroplated on Zn and melted under H_2. Cu_5Zn_8: The Zn sample was alloyed with Cu under H_2 and annealed for 2 hrs at 700°C.

$Pd\ Pb_2$: The activity was electroplated on Pd and melted under argon. The Pd sample was then alloyed with Pb, ground to powder and sealed in Araldite.

Pd_2Al: The Pd sample was alloyed with Al under argon. Cs_2PdCl_4: The Pd sample was dissolved in aqua regia and evaporated to a small volume. Concentrated CsCl solution was used to precipitate the dark yellow crystals.

^{111}Ag.

Fifty mg of Pd were irradiated for 8 hrs. at 3×10^{13} n/cm^2 sec. After 2 days cooling, the ^{111}Ag was separated in two ways: a) With carrier. The Pd was dissolved in H_2SO_4 + HNO_3 (3:1), a solution of 30 mg $AgNO_3$ was added, and AgCl was precipitated. It was dissolved in NH_3 (aq) and reprecipitated, then dissolved in KCN (aq). The Ag was electroplated onto graphite. b) Carrier free. The Pd was dissolved in conc. HCl, diluted to 12N, and passed over anion exchange resin, which retains Pd more strongly than Ag. $AgNO_3$: The ^{111}Ag

0 0 0 0 0 8 0 0 0 4 0

solution in HNO_3 was concentrated and cooled to 0°C. Ag_2SO_4: H_2SO_4 was added to the nitrate solution. K $Ag(CN)_2$: The nitrate solution was evaporated to dryness and dissolved in H_2O. From this solution Ag CN was precipitated with 0.1 N KCN. It was redissolved in an equal volume of 0.1 N KCN. The solution was concentrated and cooled to 0°C. The resulting K $Ag(CN)_2$ crystals were recrystallized from H_2O or dissolved in the solvents to be studied.

^{111m}Cd.

Two procedures were used: a) Three mg ^{110}CdO (or ^{110}Cd metal) were irradiated for 1 hr at 3×10^{13} n/cm^2 sec or alternatively 20 mg Cd (or $CdMe_2$) were irradiated for 10 min. b) Carrier-free ^{111m}Cd was produced by irradiating ^{108}Pd with 18 MeV α's and distilling off the Cd. Cd: The metal was used as irradiated, after melting, or in electroplated form. In,Tl: Approximately 0.5 mg Cd was electroplated on ∿ 100 mg In(Tl) and melted under H_2. Hg: Cd metal was dissolved under H_2 in boiling Hg. CdSb, Cd_3Ag: The metals were alloyed under H_2. $CdCl_2 \cdot 2.5H_2O$, $CdBr_2$, CdI_2, $CdSO_4 \cdot \frac{8}{3}H_2O$ $Cd(NO_3)_2 \cdot 4H_2O$: The CdO target was dissolved in HCl (HBr, HI, H_2SO_4, HNO_3), evaporated to dryness, dissolved in $CdCl_2$ ($CdBr_2$, CdI_2, $CdSO_4$, $Cd(NO_3)_2$) solution and cooled to 0°C. $CdCl_2$: The $CdCl_2 \cdot 2.5H_2O$ was heated under HCl and melted. Cd ox$\cdot 3H_2O$, K Cd $Co(CN)_6$:

The $CdSO_4$ solution was digested at ∿ 80°C with solutions of oxalic acid and $K_3Co(CN)_6$. Cd oq_2: A CdO target was dissolved in KCN (aq), and the oxyquinolate precipitated with hydroxyquinoline in KOH (aq). $K_2Cd(CN)_4$: A CdO target was dissolved in KCN. The solution was concentrated by evaporation and cooled to 0°C. $CdCO_3$: A $CdSO_4$ solution was precipitated with $NaHCO_3$ (aq). $CsCdCl_3$, $CsCdBr_3$, tma $CdBr_3$, tma_2CdBr_4: A $CdCl_2$ (Cd Br_2) solution was added to the stoichiometric amount of CsCl (CsBr, tetramethylammonium bromide) solution, evaporated and cooled to 0°C. $Cd(NH_3)_2Cl_2$: A $CdCl_2$ solution was added to NH_3 (aq) and neutralized with HCl. $Cd(CN)_2$: Solid $Cd(OH)_2$ was prepared from $CdBr_2$ solution with NaOH, dissolved in HCN and evaporated to dryness. $CdF_2 \cdot 2H_2O$, Cd $form_2 \cdot 2H_2O$: A CdO target was dissolved in HF (aq) or formic acid and evaporated to dryness. The salt was recrystallized from H_2O. $Cd(IO_3)_2 \cdot H_2O$: A $CdCl_2$ solution was added to KIO_3 (aq) and cooled to 0°C. $CsCuCl_3$: Solutions of ∿ 0.5 mg $CdCl_2$ and ∿ 100 mg $CsCuCl_3$ were combined and evaporated to a small volume. The $CsCuCl_3$ was filtered off and washed with $CsCuCl_3$ solution. Cd $tu_2(SCN)_2$, Cd tu_2Cl_2, Cd tu_4Cl_2: The thiourea salts were prepared as described in the literature (11). Cd $acac_2 \cdot MeOH$: A Cd SO_4 solution was

precipitated with sodium acetylacetonate (aq). The product was washed with H_2O, recrystallized from methanol and acetylacetone, and cooled to 0°C.

Cd Me_2: a) Cadmium dimethyl samples weighing 5-50 mg were irradiated 10-1 min with neutrons in small quartz capillaries. Each capillary was broken in vacuum, and the volatile product was distilled into a sample tube. b) A CdO sample was dissolved in HBr, evaporated to dryness and dissolved in H_2O. The solution was evaporated in vacuum, treated with CH_3MgBr in ether under argon and evaporated at -80°C. The product was distilled to a second container, and evacuated at -80°C again to drive off the remaining ether. The remaining $CdMe_2$ was distilled into the sample tube.

^{111}In.

a) A 5-mil Cd foil was irradiated with 10-40 μAh of 10 MeV protons. After cooling for one day it was dissolved in HCl. Carrier (In, La or Mg) was added, and hydroxide was precipitated with NH_3 (aq). The hydroxide was dissolved in HCl and precipitated. b) A 2-mil Ag foil was irradiated with 10 μAh of 25 MeV α particles. After cooling for a day it was dissolved in HNO_3. Bismuth carrier was added and $Bi(OH)_3$ was precipitated with NH_3 (aq). Cd: The target was used directly or after melting under H_2. In, Sn, Sb: The activity was electroplated

on Zn (In, Sn, Sb) foil, and the sample was then melted under H_2. A single crystal of Sn was obtained by slow cooling. Hg: The activity was electroplated with 1 mg of In carrier onto a tungsten wire, from which it was dissolved by boiling Hg. CdSb: The Sb sample was alloyed with Cd under H_2. InBi, In_2Bi: The $Bi(OH)_3$ containing ^{111}In was reduced in H_2 and then alloyed with In. $InPO_4$: Solid $In(OH)_3$ was dissolved in HCl and the phosphate was precipitated at ~ 80°C with Na_2HPO_4 solution.

^{181}Hf.

A 25-mg Hf sample was irradiated 1 hr at 3×10^{12} n/cm^2 sec. HfB_2, $HfSi_2$: Samples were irradiated as commercially obtained and used after 3 days cooling.

^{187}W.

A 0.1-mg W sample was irradiated 4 hrs at 6×10^{13} n/cm^2 sec or alternatively a 5 mg sample was irradiated for 6 min at 3×10^{12} n/cm^2 sec. W: A 2-mil W foil was used as commercially obtained or annealed 2 hrs at 2200°C before or after activation. Re: A 0.1 mg sample of activated W was dissolved in HF + HNO_3, evaporated to dryness and dissolved in H_2O. The solution was evaporated on a Re single-crystal disc, reduced with H_2 at 800°C and annealed 2 hrs at 2400°C in an induction furnace in vacuum.

0 0 0 0 3 8 0 0 3 5 1

^{199m}Hg.

A 20 mg sample of Hg in a quartz tube, enclosed in 5 mm BN to reduce the slow neutron contribution, was irradiated 30 min at 3×10^{13} n/cm^2 sec with reactor neutrons. Hg: The metal was used as irradiated. $HgCl_2$: Hg was dissolved in HNO_3, evaporated to dryness and dissolved in HCl. The solution was evaporated to dryness and the product recrystallized from alcohol (+ HCl). HgI_2: A stoichiometric amount of KI solution was added to the $Hg(NO_3)_2$ solution. The precipitate was recrystallized from methyl ethyl ketone.

^{204m}Pb.

Two procedures were followed: a) A 2 mil Pb foil was irradiated with 10-40 μAh of 32 MeV protons. After 4 hrs cooling it was dissolved in HNO_3, evaporated to dryness and redissolved in H_2O. Next $PbCl_2$ was precipitated with HCl at 0°C. The supernatant was evaporated and dissolved in 0.1 N HCl. The Bi activity was adsorbed on an anion exchange column and washed free of Pb. At intervals of 1-2 hrs the ^{204m}Pb produced by decay of ^{204}Bi was milked off with 0.1 N HCl. b) A 50 mg sample of pure Pb was irradiated for 1 hr at 3×10^{13} n/cm^2 sec by reactor neutrons in a 5 mm BN capsule. Pb, In, Sn, Tl: The activity was electroplated onto Pb (In, Sn, Tl) foils which were then melted under H_2.

$AuPb_2$, $PdPb_2$: The Pb metal sample was alloyed with Au(Pd) under argon. Hg: The activity was electroplated directly onto liquid Hg. $PbCl_2$: A $PbCl_2$ solution with carrier was cooled to 0°C. PbFCl, $PbSO_4$, Pb ox, $PbCrO_4$, $Pb(SCN)_2$, PbI_2: A KF(H_2SO_4, Na ox, Na_2CrO_4, Na SCN, NaI) solution was added to the $PbCl_2$ solution with carrier to precipitate the compounds. $PbBr_2$: The $PbCrO_4$ sample was dissolved in HBr, diluted, and cooled at 0°C.

^{204}Bi.

A ^{206}Pb SO_4 target was irradiated with 32 MeV protons, dissolved in conc. HCl, and worked up as for ^{204m}Pb. The pure Bi activity was stripped from the resin with conc. HNO_3. The acid was evaporated and the activity taken up in H_2O. Bi: Bi carrier was added to the solution and $Bi(OH)_3$ was precipitated with NH_3. This was reduced at 800°C with H_2. As: The solution of ^{204}Bi was evaporated on As powder, which was then annealed under H_2 at 500°C for 2 hrs. Sb: The solution of ^{204}Bi was evaporated on Sb powder, which was then melted under H_2.

0 0 0 0 0 8 0 0 0 0 2

V. NUCLEAR PROPERTIES

A. Measurements of Nuclear Spins

In contrast to magnetic dipole interactions, the electric quadrupole interaction leads to a perturbation function that is dependent on the nuclear spin. The only other factor determining this function, for a polycrystalline sample, is the asymmetry parameter. In a highly symmetric lattice a study of the perturbation function will therefore directly determine the spin of the nuclear state involved. In Figure 3 a number of examples are given to indicate the power of this unambiguous method of assigning spin values. The reason for using a polycrystalline source is illustrated by the data for $^{111}In(EC)^{111}Cd$ in Sn, as in a single crystal the observed function will depend strongly on sample orientation. While in all the cases studied in this work the previously assigned spin was confirmed, there are a number of other states of unknown spin for which this procedure might be usefully employed. One such case would be the 50 nsec state observed in the decay of ^{133}Ce (12).

B. Measurements of Nuclear Quadrupole Moments

The major difficulty in determining a nuclear quadrupole moment from a quadrupole coupling constant measured by PAC is the evaluation of the electric

field gradient in the lattice studied. There are several ways to obtain the required data, however. The most straightforward is to measure the interaction of a nucleus of known moment in the same environment. One thus measures directly the ratio of nuclear quadrupole moments and in favorable cases can connect the nuclear state studied with a calculated field gradient in an atomic state (a number that can generally be determined to an accuracy of 10%). Measurements of this type are shown in Figure 4. The calculation of field gradients in solids is usually accompanied by large uncertainties. Only in simple molecular or highly ionic structures can some confidence be placed in the results. For metals our theoretical understanding of field gradients is quite uncertain: even the sign can be in doubt. Using an electronically similar probe, however, we can at least get a rough idea about the field gradient in a simple metal, leading to an estimate of the quadrupole moment. The moments thus determined from the PAC data are summarized in Table II. They are discussed separately below.

^{44}Sc: Assuming substitutional solution of Ti in the Sc sample, the field gradient determined by NMR[13] on ^{45}Sc may be used to calculate Q(^{44}Sc) as 0.19 ± 0.02 b.

Table II. Quadrupole Moments from PAC-Studies

Lattice	Nucleus	eQq(MHz)	Reference	eQq(MHz)	Q-Ratio	Ref.-Q(b)	|Q|(b)
^{44}Ti Sc	^{44}Sc(68 keV)	1.90±0.10	^{45}Sc(g.s.)	2.02±0.03	0.94±0.05	0.22±0.01	0.21±0.02
^{99}Rh Cd	^{99}Ru(90 keV)	25.4±0.6	^{117}In(659 keV)	143±3	[0.18]	0.58±0.06	[0.10]
^{100}Pd Zn	^{100}Rh(75 keV)	11.4±0.2	^{111}Cd(247 keV)	123±2	[0.093]	[0.50]	[0.05]
^{111}In Cd	^{111}Cd(247 keV)	125±2	^{117}In(659 keV)	143±3	[0.87]	0.58±0.06	[0.50]
^{115}Cd	^{115}In(829 keV)	149±6	^{117}In(659 keV)	143±3	1.04±0.05	0.58±0.06	0.60±0.08
^{117}Cd In	^{117}In(659 keV)	21.0±0.5	^{115}In(g.s.)	30.0±0.1	0.70±0.02	0.83±0.06	0.58±0.06
^{131}Te	^{131}I(1797 keV)	409±30	^{129}I(28 keV)	373±6(η=0.8)	1,10±0.10	0.68±0.05	0.74±0.08
^{187}W Re	^{187}Re(206 keV)	376±5(300°K)	^{187}Re(g.s.)	256.2±1.0(4.2°K)	1,47±0,02	2.24±0.50	3.3±0.7
^{199m}HgCl$_2$	^{199}Hg(158 keV)	1290±80	^{201}Hg(g.s.)	708±2	1.82±0,12	0.50±0.05	0.91±0.12
^{204m}Pb Hg	^{204}Pb(1274 keV)	129	^{199}Hg(158 keV)	210±20	[0,61]	0.91±0.12	[0,56]

^{99}Ru: There is no reliable way to estimate the quadrupole moment of ^{99}Ru(90 keV) from our data. If, in a rather ambiguous way, the gradient for In in Cd (or Zn) were used, the estimate for Q would be 0.10 b. As may be seen in Figure 5, the use of the Sn or Sb data would yield quite different values.

^{100}Rh: Again the data necessary for a reliable estimate of Q(^{100}Rh, 75 keV) are not available. If, for consistency with the ^{99}Ru case, the Zn data were used, an estimate of Q ≃ 0.05 b would result.

^{111}Cd: It would be important, because of the large number of interesting experiments that can be performed with this state, to know its quadrupole moment with some accuracy. Unfortunately there is no stable Cd isotope for comparison, and the states investigated by the atomic beam technique have not been studied in a solid. Therefore one can only compare the interaction of ^{111}Cd in Cd with that of In in Cd, leading to an estimate for Q(^{111}Cd, 247 keV) of 0.50 b, quite a bit lower than assumed previously (14). This estimate, however, should be fairly reliable, as no anomalous effects are seen in Figure 5.

^{115}In: The quadrupole moment of this state may be directly calculated from the measurement in Cd to 0.60 ± 0.08 b. The measurement in Cd oxalate gave a somewhat

different value, which we prefer not to quote due to uncertainties about the structure. The size of the moment makes it very likely that the state studied is of the same type as in ^{117}In, even though the spin could not be proven unambiguously.

^{117}In: The nuclear quadrupole interaction in In metal has been determined as a function of temperature by NMR studies (15). Using the moment Q = 0.83 ± 0.06 for the ^{115}In ground state, measured by the atomic beam technique, the PAC data lead to Q = 0.58 ± 0.06 (see also (16)). This value, together with the confirmed spin of 3/2, would be in excellent agreement with the assignment of this state as the deformed [431] Nilsson state.

^{131}I: The field gradient tensor for I in Te has been determined by a Mössbauer effect study (17). The PAC measurement is not of sufficient quality for a complete analysis, but, using the asymmetry parameter of 0.8 found in Ref. (17), a moment Q = 0.46 ± 0.08 b can be determined.

^{187}Re: Since the field gradient in Re metal is well known only at 4°K (18), the quadrupole moment may be determined as Q = 3.3 ± 0.7 b if the temperature dependence is neglected. Because a Re single crystal was used, the observed pattern is different from that expected for a spin 9/2 nucleus in a polycrystalline sample. This is no serious drawback, as the spin is known with quite high reliability.

^{199}Hg: The perturbation seen in Hg Cl_2, even though not unambiguously characteristic for I = 5/2 because of time-resolution effects, may be compared with NQR data (19) to give Q = 0.85 ± 0.12 b. The quite close agreement of this value with an earlier time-integral PAC investigation (20) appears fortuitous as the interactions found in Hg metal disagree strongly.

^{204}Pb: It is not possible to determine the moment of this state from the data obtained so far. If one uses the field gradient measured for Hg in Hg metal, a rough estimate of 0.50 b can be made.

VI. RESULTS

A. Measurements in Metals

In all the cases studied, the perturbations found in metals may be considered representative of the equilibrium electronic environment. Only the lattice position of the atom should be dependent on the parent used. For the especially important hcp lattice the field gradients observed are directly related to the deviation of the c/a ratio from the ideal value of 1.633. PAC measurements are uniquely suited for measurements of field gradients in metals, since RF-techniques are hampered by the skin effect. PAC also has the possibility of measuring extremely small concentrations. As a general rule it may be expected that metals with structures strongly deviating from cubic will present large field gradients to all solute atoms. This would lead to a roughly linear relationship between the interactions of two atoms measured in a number of lattices. In Figure 5 the data in metals are displayed to show this general trend. Points deviating strongly from the expected trend could be indicative of non-substitutional solution. One can gain only a qualitative insight into the magnitude of field gradients in metals in this way. It would be very useful if the signs of the interaction could be determined in some

representative cases to clarify the contributions of conduction electrons relative to ionic charges (21).

For alloys the interpretation of the measured field gradients is even more complicated. In favorable cases it will be possible, however, to determine the site of an impurity taken up in an alloy. The experimental results obtained in metallic lattices are summarized in Table III. The field gradients are interpreted below.

^{44}Ti(EC)^{44}Sc: The small field gradient for Sc in Sc, found in NMR experiments, reflects the small hexagonal distortion of the Sc lattice. Measurements in the very similar rare-earth lattices would be of interest.

^{99}Rh(EC)^{99}Ru: The field gradients measured for Ru in metals are complicated by the possible contributions of localized electrons (in the case of Cd, Zn, and Sn) and non-substitutional solution (in the case of Sb). The small field gradient in Ru metal found by Mössbauer measurements (22) in confirmed.

^{100}Pd(EC)^{100}Rh: The quite similar field gradients for Rh in Zn and the alloys Pd_2Al, $PdPb_2$, and Cu_5Zn_8 could be indicative of the dominant contribution of localized electrons in this case. The small interaction frequency for Ru metal, however, probably reflects the small distortion of the lattice.

Table III. Results in Metallic Lattices. Errors in Last Place are given in Parenthesis

Parent	Daughter	Lattice	eQq(MHz)	A_2^{eff}	τ_2(nsec)
^{44}Ti	^{44}Sc(68 keV)	Sc	1.90(10)	+0.03	--
^{99}Rh	^{99}Ru(90 keV)	Ru	2.7 (5)	-0.18	--
"	"	Zn	21.0 (10)	-0.10	60
"	"	Cd	25.4 (6)	-0.10	> 500
"	"	Sn	24.0 (15)	-0.10	40
"	"	Sb	79.0 (20)	-0.05	30
^{100}Pd	^{100}Rh(75 keV)	Zn	11.4 (2)	+0.14	1500
"	"	Ru	1.0 (3)	+0.08	--
"	"	Cu_5Zn_8	10.6 (15)	+0.14	300
"	"	Pd_2Al	15.0 (5)	+0.08	>2000
"	"	$PdPb_2$	10.0 (3)	+0.16	800
^{111m}Cd	^{111}Cd(247 keV)	Cd	125.0 (20)	+0.12	--
"	"	In	17.3 (3)	+0.12	--
"	"	Hg	110.0 (10)	+0.12	--
"	"	Tl	7.8 (8)	+0.12	--
"	"	CdSb	111.0(30)(η = 0.5)	+0.05	--

(continued)

Table III (continued)

Parent	Daughter	Lattice	eQq(MHz)	A_2^{eff}	τ_2(nsec)
^{111m}Cd	^{111}Cd(247 keV)	Cd_3Ag	36.2(δ = 50%)	+0.10	--
^{111}In	^{111}Cd(247 keV)	Zn	123.0 (10)	-0.11	>1000
"	"	Cd	126.0 (10)	-0.05	--
"	"	Hg	112.0 (10)	-0.11	>2000
"	"	Ga(77°K)	23.8(δ = 5%)	-0.10	--
"	"	In	17.3 (2)	-0.11	>2000
"	"	In(77°K)	24.4 (3)	-0.11	>2000
"	"	Sn	36.0 (3)	-0.11	>2000
"	"	Sb	70.7 (10)	-0.03	--
"	"	Bi	302.0 (30)	-0.04	150
"	"	In(plated)	7.8(δ = 10%)	-0.13	--
"	"	CdSb	139.0(2.5)(η = 0.3)	-0.07	--
"	"	AuIn	63.4(10)(η = 0.3)	-0.08	--
"	"	InBi	11.2 (3)	-0.15	--
"	"	InBi(77°K)	8.3 (3)	-0.15	--
"	"	In_2Bi	40.0 (5)	-0.07	--
"	"	In_2Bi(77°K)	51.3 (5)	-0.08	--
^{115}Cd	^{115}In	Cd	149 (6)	0.06	--

(continued)

Parent	Daughter	Lattice	eQq(MHz)	A_2^{eff}	τ_2(nsec)
^{117}Cd	^{117}In	In	21.0(5)	-0.19	--
"	"	Cd	143 (3)	-0.11	--
"	"	Sn	[62]	-0.16	--
^{131m}Te	^{131}I(1797 keV)	Te	409(30)(η = 0.80)	+0.09	--
^{181}Hf	^{181}Ta(482 keV)	HfB_2	350 (10)	-0.15	100
"	"	$HfSi_2$	129(5)(δ = 5%)	-0.12	--
^{187}W	^{187}Re(206 keV)	Re	376 (6)	-0.04	400
"	"	W(cold worked)	--	-0.06	54(15)
"	"	W(annealed before(n,γ))	--	-0.07	172(30)
"	"	W(annealed after(n,γ))	--	-0.07	183(30)
^{199m}Hg	^{199}Hg(158 keV)	Hg	210 (20)	+0.14	--
^{204m}Pb	^{204}Pb(1274 keV)	Cd	[118]	+0.12	800
"	"	In	41 (1)	+0.15	>1000
"	"	Sn	71.2 (15)	+0.18	>2000
"	"	Hg	[129](δ = 10%)	+0.08	--
"	"	Tl	13.4 (3)	+0.18	--
"	"	$PdPb_2$	187 (5)	+0.12	--

(continued)

Table III (continued)

Parent	Daughter	Lattice	eQq(MHz)	A_2^{eff}	τ_2(nsec)
^{204}Bi (^{204m}Pb)	^{204}Pb(1274 keV)	As	65.0 (15)	+0.08	--
"	"	Sb	33.3 (10)	+0.10	--
"	"	Bi	17.5 (5)	+0.08	--
^{204}Bi	"	Bi	17.9 (8)	-0.05	--

^{111}Ag(β^-)^{111}Cd: Due to the cubic structure of Ag, the unperturbed correlation was found in Ag metal.

^{111}Cd(IT)^{111}Cd: For Cd and In the results, taken together with those of the ^{111}In decay, prove substitutional solubility. This is also extremely likely for Tl and Hg. When a Cd concentration in Tl above the solubility limit was used, a second interaction, showing Cd metal, was superimposed on the curves for Cd in Tl. The alloy Cd_3Ag shows a large frequency spread, probably due to disorder in the crystal.

^{111}In(EC)^{111}Cd: The data for Zn, Cd, and Hg show the strong distortion of the crystal lattice, while Ga, In, and Tl, though they have different structures, all show effectively cubic site symmetry. Indium metal produced by electrolysis shows a different perturbation from melted material, indicating an incomplete crystallization. In the cases of Sn and Sb hosts, the In activity cannot be definitely assumed to occupy a substitutional site, while for Bi this is likely not to be the case, accounting for the different results obtained with different sample preparation. If these points are excluded from Figure 5, a reasonable consistency is found. The non-equivalence of the ^{111m}Cd and ^{111}In data in CdSb

prove that In dissolved in CdSb is not at Cd sites. InBi shows an unusual temperature dependence, while In_2Bi has the normal behavior. Many more In alloys like these or AuIn could be studied by PAC with high accuracy.

$^{115}Cd(\beta^-)^{115}In$: The interaction in Cd metal shows the same large field gradient found for ^{111}Cd in this lattice.

$^{117}Cd(\beta^-)^{117}In$: The interactions observed in Cd and In are as expected from the ^{111}Cd data. The fairly large quadrupole coupling constant in Sn shows (as do the data of Pb and Ru in Sn) that the interaction found for ^{111}Cd in Sn is unusually small.

$^{131m}Te(\beta^-)^{131}I$: Mössbauer effect experiments have shown that the site observed for I after β decay from Te is not substitutional.

$^{181}Hf(\beta^-)^{181}Ta$: The alloys HfB_2 and $HfSi_2$ show quite large field gradients, as should be expected from their structure. The frequency spread in $HfSi_2$ is probably due to the crystalline imperfections of the commercial material rather than to damage introduced by the neutron irradiation.

$^{187}W(\beta^-)^{187}Re$: The high accuracy of the measurement in Re metal should make further experiments on the temperature dependence feasible. This might clear

up the discrepancies between specific heat and acoustic resonance data in Re. The strong effect of annealing, independent whether it was done before or after neutron irradiation, shows that the attenuation observed in commercial W metal is due to the lattice defects introduced in cold working.

^{199m}Hg(IT)^{199}Hg: The field gradient in Hg metal measured by PAC should make a search for the NQR absorption of ^{201}Hg in this metal possible. The value measured is quite different from a previous time integral experiment.

^{204m}Pb(IT)^{204}Pb: The field gradients found for the Tl, In, Sn, Hg, and Cd lattices reflect the general trend found in the ^{111}Cd data. They therefore are probably characteristic of substitutional sites. Alloys like $PdPb_2$ are easily studied.

^{204}Bi(EC)^{204}Pb: The data in Bi, Sb, and As are representative for Pb atoms at substitutional sites in these lattices. They reflect the stronger covalence in Sb and especially As.

B. Measurements in Insulators

1. General Observations

The investigation of solid insulators by PAC are complicated by several factors. These may be classified according to the kind of decay preceding the observed γ-γ cascade. Representative examples for the three decay modes studied in insulators are shown in Figure 6.

a. Isomeric decay. For the cases studied (^{111}Cd, ^{204}Pb, ^{199}Hg) no effects attributable to the perturbation of the atomic environment have been found. This is to be expected because of the small (< 1 eV) recoil energy of an isomeric transition. The observed interaction therefore may be considered representative for the site taken up by the nucleus before the decay. For most insulating solids, however, the site symmetry is not high enough to fix the directions of the major axes of the FGT. Even fewer are the cases of trigonal or tetragonal site symmetry, so that a non-vanishing asymmetry parameter ($\eta \neq 0$) is found in most instances. Figure 7 shows two examples for the resulting type of perturbation. Only if a field gradient of molecular origin is very strong may the perturbation due to the crystalline environment be neglected (e.g. in $Cd(CH_3)_2$ or $Hg\ Cl_2$), resulting in almost axial symmetry. The requirement of using a macroscopically isotropic source are especially important in determining the asymmetry parameter. In principle measurements of the orientation dependence in single crystals could be employed to find the FGT axes, but it would be preferable to perform this experiment with an externally applied magnetic field, studying the combined interaction.

0 0 0 0 0 3 8 0 0 0 5 0

b. β^--decay: PAC experiments after β-emission in a number of cases (^{111}Ag, ^{117}Cd, ^{181}Hf) have shown that a well-defined field gradient exists after the β^- process for a large portion (80-90%) of the nuclei formed. There is little doubt that these occupy the site of the parent. There is somewhat less certainty about the charge state of the resulting ion, however. Shake-off events accompanying β-decay may result in very high charge states, but they will occur only in a small fraction of ions, so that for most ions only one electron will be lost. In the cases investigated so far, the resulting charge state ($\Delta Z = +1$) of the daughter ion is chemically stable and is probably the one observed in PAC. No time-dependent effects arising from the preceding nuclear decay are therefore expected, in accordance with the experimental results. As an impurity atom is being studied, however, the interpretation of such results is much less straightforward than in the case of isomeric-state decay.

A similar situation is expected for β^+ decay, but no PAC experiments have been performed with a source in which β^+ decay dominates over EC-decay. Several measurements with EC-sources have been reported in which the primary decay leads to a fairly long-lived state in the daughter nucleus, which then

decays through the γ-γ cascade (^{44}Ti, ^{120}Sb). A stable charge state may be established during the lifetime of the long-lived state, leading to a situation similar to isomeric-state decay. The charge of the ion in this case will be influenced by the chemical environment as well as the nature of the atom itself. No general predictions may be made about which stable charge state will be observed experimentally. Any conclusion about the host material drawn from such experiments will be of even higher uncertainty than for the case of β^- decay.

c. Electron-capture decay: Some of the cases best suited for PAC experiments are cascades fed by EC-decay (^{99}Rh, ^{100}Pd, ^{111}In). For ionic solids these show markedly similar behavior. The anisotropy is attenuated strongly in a comparatively short time and no periodic modulation is found. This attenuation could in principle have several origins. As it does not occur in metals, the extremely fast ($< 10^{-12}$ sec) effects of the holes formed in the inner electron shells or the following Auger process may be neglected. After these events, however, the ion is left in one of a number of possible unstable charge states. These, together with possible electronic defects in the atomic environment, will lead to a wide spread of interaction frequencies. The interaction of the ion with the environment should change with time, although experiments with ^{111}In failed

0 0 0 0 3 8 0 0 0 6 1

to show this time dependence (23). The major influence of the surrounding on the nucleus after EC decay appears to be the electric quadrupole interaction, although magnetic perturbation cannot be excluded.

It appears that in general PAC experiments after EC in insulating solids will be strongly affected by the influence of the radioactive decay. They appear to be more suited to studying the charge states produced than the structure of the specific solid under investigation. As expected, however, there are slightly different perturbations in different solids, suggesting that the lattice has some influence. Perhaps the study of semiconductors could help resolve the uncertainties about these phenomena.

2. Detailed Results.

Results for solid insulators are given in Table IV. They are discussed below.

^{99}Rh(EC)^{99}Ru: A strongly damped correlation was found in the Rh complex $Rh(NH_3)_3Cl_3$.

^{100}Pd(EC)^{100}Rh: In Cs_2PdCl_4 the same behavior, characteristic of EC decay, was found. The observed perturbation could be fitted by a simple exponential.

Table IV. Results in Insulating Solids. Errors are given in Parenthesis

Parent	Daughter	Lattice	eQq(MHz)	η	A_2^{eff}	τ_2^{eff}(nsec)
^{99}Rh	Ru(90 keV)	$Rh(NH_3)_3Cl_3$	--	--	-0.10	6
^{100}Pd	^{100}Rh(75 keV)	Cs_2PdCl_4	--	--	+0.10	15
^{111}Ag	^{111}Cd(247 keV)	$AgNO_3$	113 (2)	0.25	-0.10	>1000
"	"	Ag_2SO_4	91 (3)	0.95	-0.09	>1000
"	"	$AgBrO_3$	[42]	0	-0.07	500
"	"	$KAg(CN)_2$	550 (10)	0.0	-0.07	>2000
^{111m}Cd	^{111}Cd(247 keV)	$CdCl_2$	48.7 (10)	0.0	+0.10	--
"	"	$CdBr_2$	24.6 (5)	0.0	+0.16	
"	"	CdI_2	9.7 (8)	0.0	+0.14	
"	"	$CsCdCl_3$	16.7 (10)	0.0	+0.12	400
"	"	$CsCdBr_3$	18.3 (5)	0.0	+0.14	--
"	"	$N(CH_3)_4CdBr_3$	35.5 (5)	0.0	+0.12	--
"	"	$[N(CH_3)_4]_2CdBr_4$	17.0 (5)	0.8	+0.11	--
"	"	$Ce_2Mg_3(NO_3)_{12}\cdot 24H_2O$	--	--	+0.13	200
"	"	$K_2Cd(CN)_4$	0.0	--	+0.13	>1000
"	"	$CdF_2\cdot 2H_2O$	39.4 (10)	0.75	+0.10	--

(continued)

0 0 0 0 3 8 0 0 0 6 3

$Cd(thiourea)_2Cl_2$, and $Cd(thiourea)_2(SCN)_2$ reflect the strong differences of the two coordinating ligands in each case. Cadmium in $CsCuCl_3$ is an interesting case, as the large field gradient and asymmetry parameter clearly show the strong distortion from octahedral coordination in this compound. The large interaction frequencies observed in $KCdFe(CN)_6$ and $Cd_3(Co(CN)_6)_2$ should be interpreted as indicating a highly asymmetric environment of the Cd ions in these lattices. The spread in frequencies observed for CdS and $CdCO_3$ shows the strongly imperfect crystal structure obtained for these compounds on precipitation, while in $Cd(thiourea)_4Cl_2$, $Cd(acetate)_2$, and $Cd(acetylacetonate)_2 \cdot CH_3OH$ a plausible explanation would involve more than one lattice site of the Cd ions. Further investigation of the strong decrease of the observed perturbation in $Cd(CN)_2$ is planned. The large field gradient found for $Cd(CH_3)_2$ is clearly of molecular origin, as evidenced by the frozen solutions in ether and tetrahydrofurane, which show the static interaction of isolated molecules. Damping of the perturbation in this case is probably due to a frequency spread induced by the matrix, rather than molecular motion at 77°K.

$^{111}In(EC)^{111}Cd$: The perturbation found in $InPO_4$ is of the type well known for this decay. It was fitted with a spread of interaction frequencies and an exponential relaxation.

$^{115}Cd(\beta^-)^{115}In$: The data in Cd (oxiquinolate)$_2$ show a very strong field gradient, similar to ^{111}Cd in this lattice. The same is true for the Cd oxalate sample.

$^{117}Cd(\beta^-)^{117}In$: The attenuation observed in Cd oxalate is probably not due to the preceding β-decay, as the perturbation found in $Cd(NO_3)_2 \cdot 4H_2O$ is not attenuated.

$^{199m}Hg(IT)^{199}Hg$: The strong field gradients measured for $HgCl_2$, Hg_2Cl_2, and $Hg(CH_3)_2$ are an indication of the highly covalent nature of the bonding in these compounds. The crystal structure of HgI_2 is not of the molecular type, leading to a comparatively small field gradient.

$^{204m}Pb(IT)^{204}Pb$: The field gradients observed for the halides PbFCl, $PbCl_2$, and PbI_2 reflect the distortion of the ionic coordination. The spread of interaction frequencies found in PbFCl is possibly due to disorder in the crystal. The difference between the isostructural $PbSO_4$ and $PbCrO_4$ shows the sensitivity of the nuclear quadrupole interaction to small structure changes.

Table V. Results in Solutions

Parent	Daughter	Solution	A_2^{eff}	τ_2^{eff}(nsec)
^{99}Rh	^{99}Ru(90 keV)	2N H_2SO_4	-0.14	> 500
^{111}Ag	^{111}Cd(247 keV)	2N HNO_3	-0.13	>2000
"	"	$KAg(CN)_2$ in H_2O	-0.12	30 (3)
"	"	$KAg(CN)_2$ in H_2O (100°C)	-0.07	134 (15)
"	"	$KAg(CN)_2$ in 0.6N KCN	-0.10	> 650
"	"	$KAg(CN)_2$ in 10N KCN	-0.12	> 500
"	"	$KAg(CN)_2$ in acetone	-0.11	53 (5)
"	"	$KAg(CN)_2$ in H_2O:glycerine(1:1)	-0.12	4 (1)
"	"	$KAg(CN)_2$ in H_2O:glycerine(2:1)	-0.13	8 (2)
"	"	$KAg(CN)_2$ in H_2O:glycerine(3:1)	-0.08	19 (3)
^{111m}Cd	^{111}Cd(247 keV)	$Cd(CH_3)_2$(0°C)	+0.10	20 (3)
"	"	$Cd(CH_3)_2$	+0.13	52 (6)
"	"	Cd in THF	+0.14	55 (8)
"	"	Cd in ether	+0.14	90 (10)
^{111}In	^{111}Cd(247 keV)	2N HNO_3	-0.13	>1000

(continued)

Table V (continued)

Parent	Daughter	Solution	A_2^{eff}	τ_2^{eff}(nsec)
^{181}Hf	^{181}Ta(482 keV)	2N HF	-0.20	> 260
^{187}W	^{187}Re(206 keV)	2N HF	-0.06	20 ± 5
^{204}Bi	^{204}Pb(?)	2N HCl	+0.08	>4000
"	"	2N HCl	-0.04	>4000
^{204m}Pb	^{204}Pb(1274 keV)	2N HCl	+0.16	>2000

to the presence of a second 912 keV γ ray in this decay and possibly also due to some contribution of the 984-keV line in the energy window. The anisotropy of the 984-375 keV cascade is in agreement with the I=5 assignment for the 2258 keV level (24).

D. Measurements in Gases

Molecular motion in gases is of the simplest kind. It would be a valuable check of PAC theory if a systematic study could be made. Obviously the simplest situation would be presented by a diatomic molecule with a nucleus decaying through an isomeric transition. The linear molecule dimethylcadmium, $Cd(CH_3)_2$, is similar to such a case. Preliminary attempts to study the isolated molecule at a pressure low enough to make the time between collisions long compared to the lifetime of the intermediate state have failed for experimental reasons. It has been possible, however, to study the attenuation of the angular correlation in the presence of a variety of collision partners. All experiments were performed at constant pressure (1.5 atm) and at room temperature. Under these conditions the collision frequency is much lower than the molecular rotation frequency. Therefore the field gradient acting on the nucleus is the component

along the rotation axis, $q_{eff} = -\frac{1}{2} q_{mol}$. (At higher pressures this would no longer hold. A nonlinear pressure dependence of the relaxation time is therefore expected.) Table VI summarizes the results obtained. For the noble gases a decrease in mass leads to an increased collision frequency. This results in a shorter correlation time, a trend reflected by the increase in relaxation time from Xe to Ne. The sharp drop observed for He shows the breakdown of the strong collision model. The same effect can be seen for H_2 and D_2. The small momentum transferred by the light gases on one collision is not sufficient to randomize the molecular rotation axis. The theoretical points in Figure 9 represent the simple strong collision model for the noble gases. The collision frequencies $1/\tau_{coll} = \overline{V}/\Lambda$ have been calculated from the average velocity $\overline{V} = \sqrt{3kT(1/m_1 + 1/m_2)}$ and the mean free path $\Lambda = kT/p\pi(r_1 + r_2)^2$, using a collision radius of $r_1 = 4$ Å for $Cd(CH_3)_2$.

0 0 0 0 3 8 0 0 0 6 4

A partial covalency of the bonding in Pb oxalate and $Pb(SCN)_2$ leads to fairly large field gradients. The large asymmetry of the ionic environment in the structure of tetragonal PbO can explain the high interaction frequency.

C. Measurements in Liquids

For metallic liquids the same conclusions as for solid metals should hold, leading to long nuclear relaxation times. The situation in ionic liquids is quite different from solids, however. Rapid rotational motion averages the local field gradient at the nucleus. Any perturbation of the nuclear environment is annealed in a very short time, so that the ion may be considered in its normal charge state. For this reason the nuclear relaxation observed in PAC is equivalent to that observed in NMR, leading in most cases to an unperturbed correlation. In molecular solutions effects of the preceding decay similar to those in solids are expected. For isomeric or β decay the motion of the molecular species produced will be the major effect influencing the observed perturbation. If the strength of the nuclear quadrupole interaction in the molecular complex is known, an analysis of the perturbation (usually a simple exponential decay) will give the rotational correlation time.

An example for such a case is shown in Figure 8. The use of a cascade

populated by EC decay for such a measurement, however, is not as straightforward, as the approach of the environment to charge equilibrium must also be considered. The experimental results in solutions are summarized in Table V.

$^{111}Ag(\beta^-)^{111}Cd$: In HNO_3 solution the full anisotropy expected for this cascade is found. The attenuations observed for solutions of the $Ag(CN)_2^-$ complex in H_2O (100°C), acetone, H_2O, and H_2O-glycerine (3:1, 2:1, 1:1) are strongly correlated with the viscosity of the solvent. The rotational correlation times can be calculated from these data. The unperturbed correlation in the 10M KCN solution can be explained by the presence of the symmetrical $Ag(CN)_4^{3-}$ complex, but in 0.6M KCN the $Cd(CN)_4^{2-}$ complex has to be formed after the decay, since in such a solution the $Ag(CN)_2^-$ ion is still the dominant species.

$^{111m}Cd(IT)^{111}Cd$: The attenuations found for $Cd(CH_3)_2$ in ether, tetrahydrofurane, $Cd(CH_3)_2$, and $Cd(CH_3)_2$(0°C) vary as expected from the viscosities of the solvents.

$^{187}W(\beta^-)^{187}Re$: The observed correlation in HF_{aq} is strongly attenuated. The dependence of this effect on HF concentration should give more information about what complex is present in solution.

$^{204}Bi(EC)^{204}Pb$: No perturbation was observed in HCl solution. The anisotropy of the 912-375 keV cascade was reduced below the effect of the ^{204m}Pb decay owing

Table VI. Results for ^{111m}Cd dimethyl in various gases

Buffer gas (1.5 atm)	A_2^{eff}	$1/\lambda_2$(ns)	τ_c^{eff}(ns)	τ_{coll}(ns)
H_2	0.13	10 ± 3	0.17	0.017
D_2	0.11	19 ± 4	0.09	0.024
He	0.10	20 ± 4	0.09	0.026
Ne	0.11	45 ± 7	0.04	0.049
Ar	0.11	30 ± 5	0.06	0.061
Kr	0.11	2.9 ± 4	0.06	0.074
Xe	0.11	26 ± 4	0.07	0.082
CH_4	0.11	33 ± 4	0.05	0.041
N_2	0.12	36 ± 5	0.05	0.051
CO	0.11	33 ± 5	0.05	0.051

VII. CONCLUSIONS

Perturbed γ-γ angular correlations may be used to study the nuclear quadrupole interaction in a wide variety of samples. As the theory is well developed, this technique provides a powerful tool for investigating the extranuclear environment. The possibility of using trace quantities is an important advantage of PAC. Especially in metals it can compete favorably with other techniques. The growing number of accurate measurements should lead to a detailed understanding of electric field gradients in metals in the near future.

If an isomeric state of the nucleus under study may be used as a source (as in Cd, Hg, Pb), insulators can be studied with the same reliability. Some care must be exercised in interpreting data obtained with β-emitters on insulating samples, while the use of an electron-capture source will give information mainly about the disruption of the nuclear environment produced by the decay. Measurements on liquids or gases are of particular interest for studying molecular motion.

ACKNOWLEDGMENTS

Mrs. Winifred Heppler is gratefully acknowledged for a great deal of very valuable assistance in all phases of the chemical preparations. H.H. was supported during part of this work by a NATO Fellowship.

0 0 0 0 5 8 0 0 0 6 7

FOOTNOTES AND REFERENCES

*Work performed under the auspices of the U. S. Atomic Energy Commission.

(1) H. Frauenfelder and R. M. Steffen, in Alpha-, Beta-, and Gamma-Ray Spectroscopy, K. Siegbahn, ed., Vol. 2, p. 997 (North Holland, 1965). This comprehensive review describes PAC theory and experiments, with numerous references.

(2) A. Abragam and R. V. Pound, Phys. Rev. 92, 943 (1953).

(3) P. da R. Andrade, J. D. Rogers, and A. Vasques, Phys. Rev. 188, 571 (1969).

(4) D. Dillenburg and Th. A. J. Maris, Nucl. Phys. 33, 208 (1962).

(5) A. G. Marshall and C. F. Meares, J. Chem. Phys. 56, 1226 (1972).

(6) R. M. Lynden-Bell, Molec. Phys. 21, 891 (1971).

(7) M. Blume, Nucl. Phys. A167, 81 (1971).

(8) D. A. Shirley, J. Chem. Phys. 55, 1512 (1971).

(9) E. Matthias, S. S. Rosenblum, and D. A. Shirley, Phys. Rev. 139, B532 (1965).

(10) J. S. Evans, E. Kashy, R. A. Naumann, and R. F. Petry, Phys. Rev. 138, B9 (1965).

(11) Garr. Chim. Ital. 86, 867 (1956), ibid. 87, 137 (1957), ibid. 87, 917 (1957).

(12) C. Gerschel, N. Perrin, and L. Valentin, Phys. Letters 33B, 299 (1970).

(13) R. G. Barnes, F. Borsa, S. L. Segel, and D. R. Torgeson, Phys. Rev. 137, A1828 (1965).

(14) H. J. Behrend and D. Budnick, Z. Physik. 168, 155 (1962).

(15) R. R. Hewitt and T. T. Taylor, Phys. Rev. 125, 524 (1962).

(16) R. S. Raghavan and P. Raghavan, Phys. Rev. Letters 28, 54 (1972).

(17) M. Pasternak and S. Bukshpan, Phys. Rev. 163, 297 (1967).

(18) P. E. Gregers-Hansen, M. Krusius, and G. R. Pickett, Phys. Rev. Letters 27, 38 (1971).

(19) H. G. Dehmelt, H. G. Robinson, and W. Gordy, Phys. Rev. 93, 480 (1954).

(20) R. V. Pound and G. K. Wertheim, Phys. Rev. 102, 396 (1956).

(21) R. E. Watson, A. C. Gossard, and Y. Yafet, Phys. Rev. 140, A375 (1965).

(22) O. C. Kistner, S. Monaro, and R. Segnan, Phys. Letters 5, 299 (1963).

(23) F. Falk, A. Linnfors, and J. E. Thun, Nucl. Phys. A152, 305 (1970).

(24) Nucl. Data Sheets B5, 601 (1971).

FIGURE CAPTIONS

Fig. 1. Level scheme of ^{111}Cd.

Fig. 2. Diagram of 4-detector system (a) and schematic of slow coincidence unit (b). (UV = univibrator).

Fig. 3. Spin dependence of the perturbation function with axially symmetric field gradient. Data and theoretical curves are shown for each case.

Fig. 4. Examples of the measurement of nuclear quadrupole moments by PAC.

Fig. 5. Quadrupole coupling constants for ^{111}Cd (247 keV) in several non-cubic metals compared to those of some other nuclei.

Fig. 6. Typical perturbations observed in insulators for isomeric state decay, β-decay, and EC-decay.

Fig. 7. Examples of the perturbations observed in the case of non-axially symmetric field gradients.

Fig. 8. Comparison of the influence of the nuclear quadrupole interaction in solid and liquid.

Fig. 9. Effect of different gases on the relaxation time in Cd $(CH_3)_2$. The theoretical curve is for the case of strong collisions.

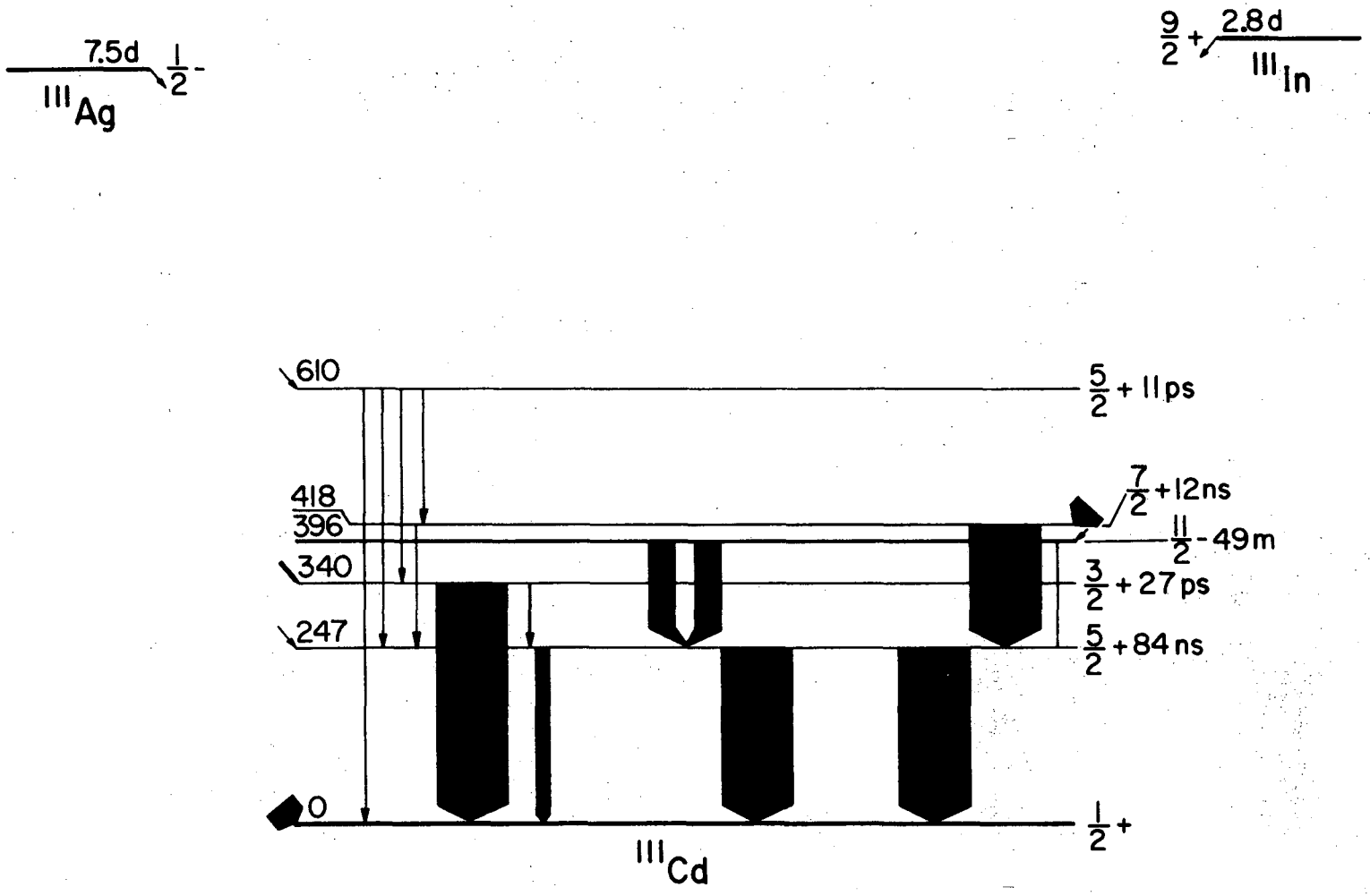
7.5d
1/2-
111Ag
9/2+
2.8d
111In
610
5/2+ 11ps
418
396
7/2+ 12ns
11/2- 49m
340
3/2+ 27ps
247
5/2+ 84ns
0
1/2+
111Cd
XBL7212-4928

Fig. 1

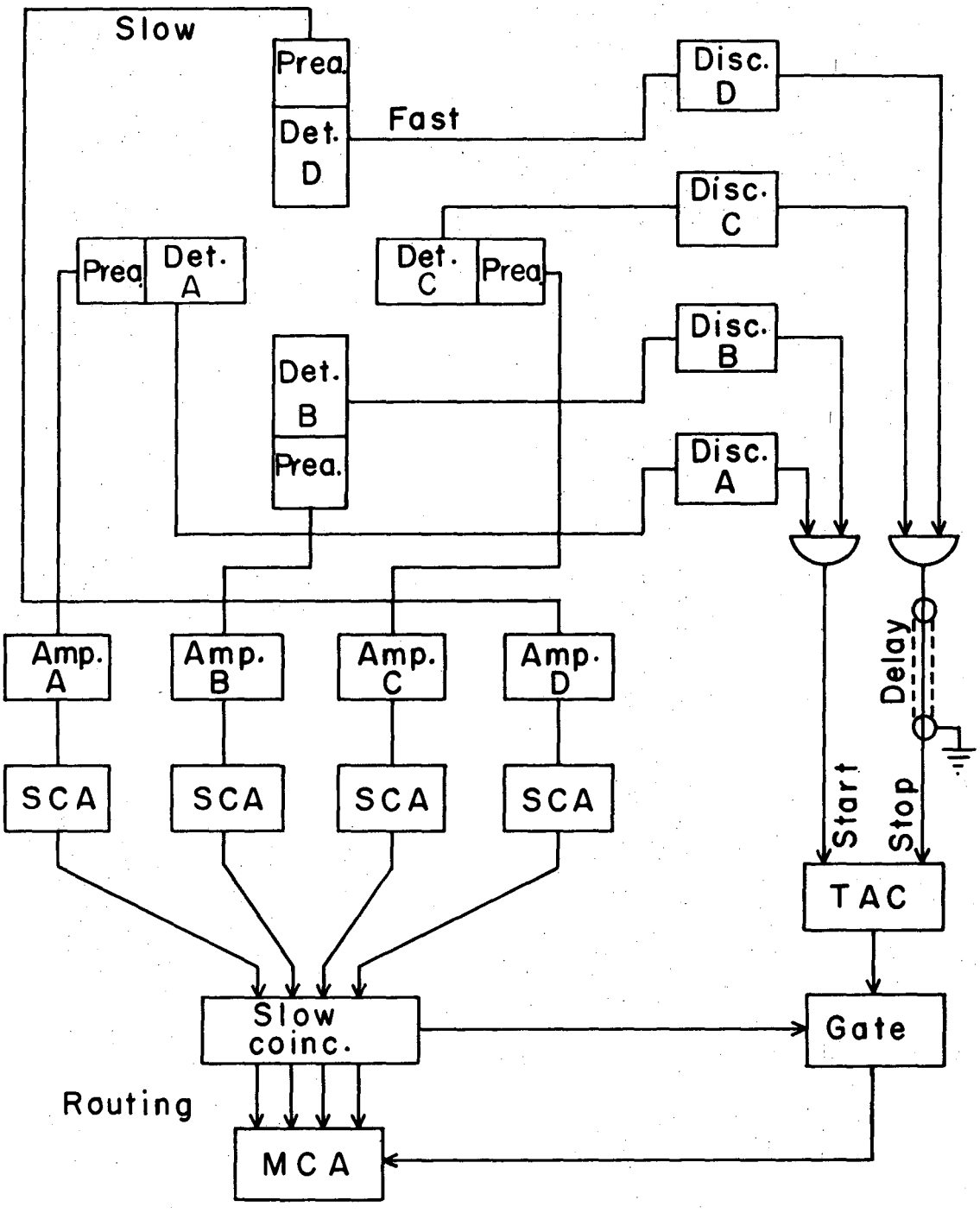
Slow
Prea.
Det. D
Fast
Disc. D
Disc. C
Det. C
Prea.
Prea.
Det. A
Det. B
Prea.
Disc. B
Disc. A
Amp. A
Amp. B
Amp. C
Amp. D
Delay
SCA
SCA
SCA
SCA
Start
Stop
TAC
Slow coinc.
Gate
Routing
MCA
XBL.714-3246

Fig. 2a

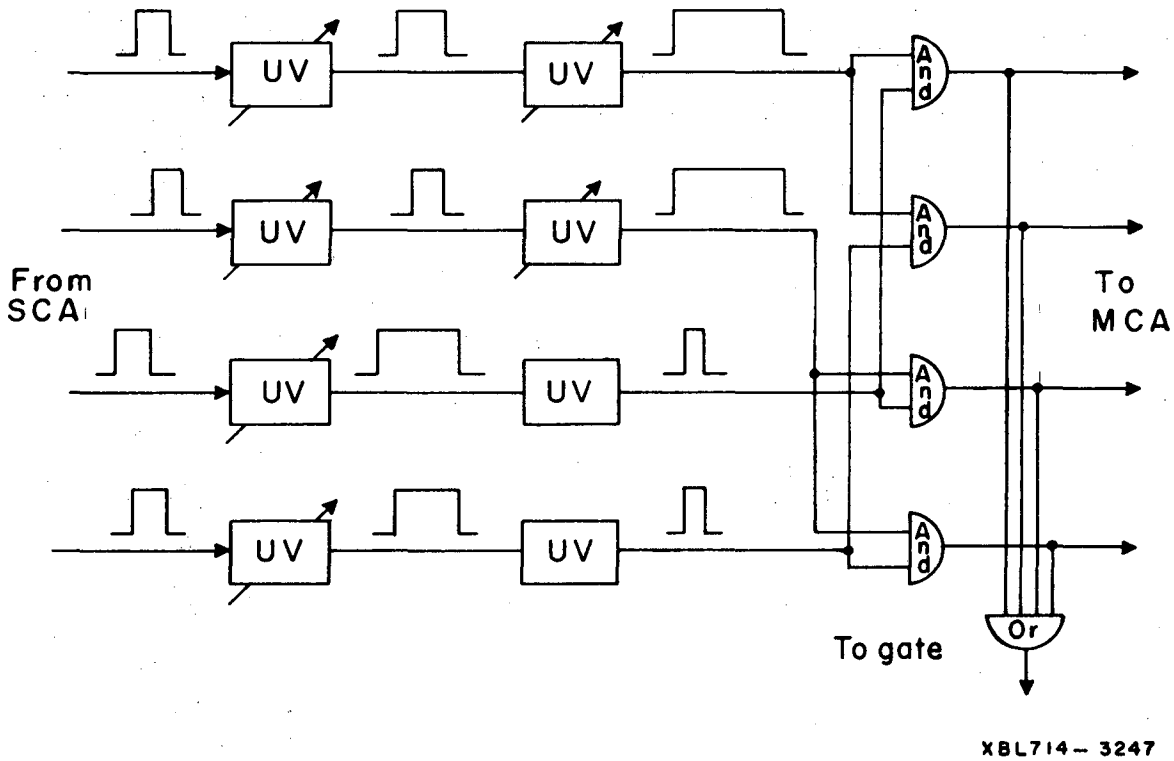
UV
UV
UV
UV
UV
UV
UV
UV
And
And
And
And
Or
From SCA
To MCA
To gate
XBL714-3247

Fig. 2b

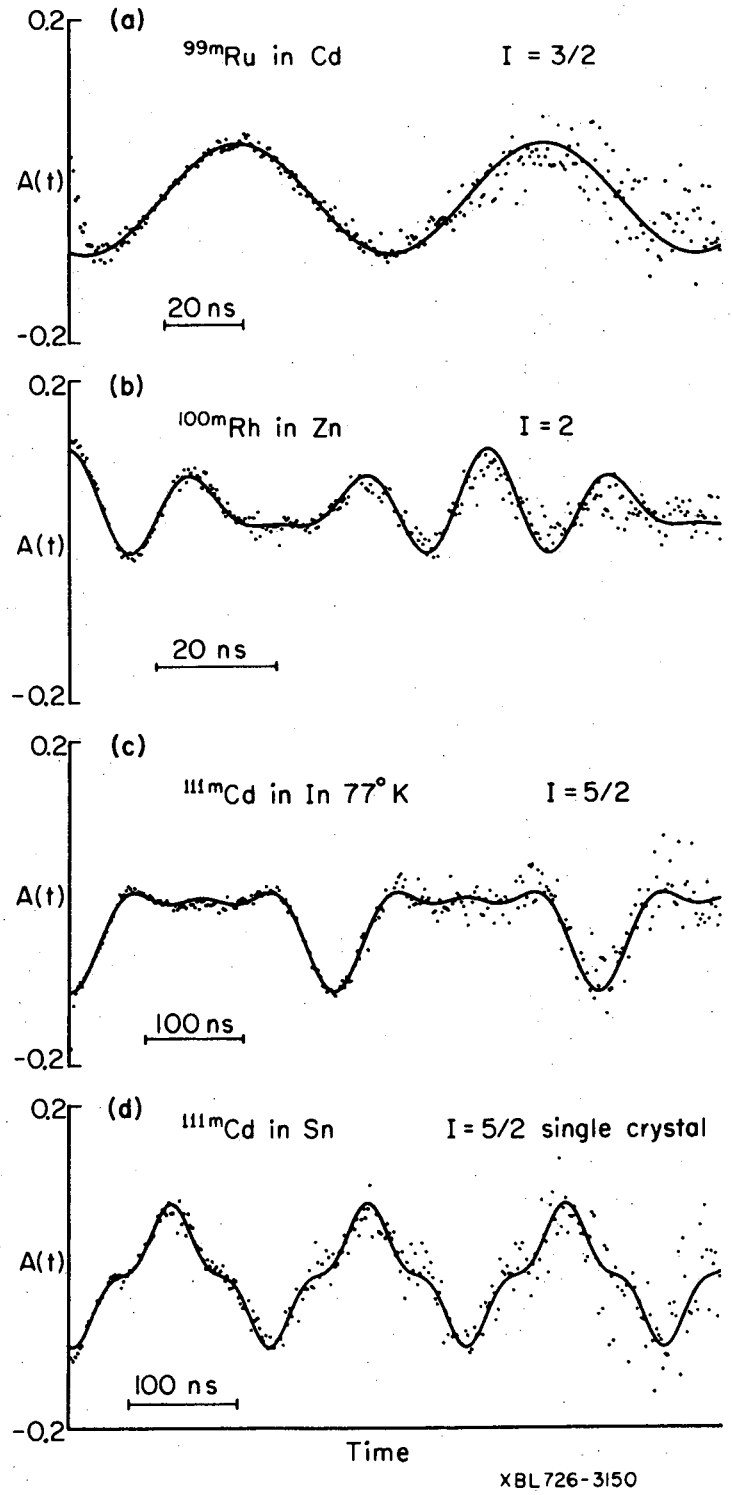
0.2
(a)
^{99m}Ru in Cd
I = 3/2
A(t)
20 ns
-0.2
0.2
(b)
^{100m}Rh in Zn
I = 2
A(t)
20 ns
-0.2
0.2
(c)
^{111m}Cd in In 77° K
I = 5/2
A(t)
100 ns
-0.2
0.2
(d)
^{111m}Cd in Sn
I = 5/2 single crystal
A(t)
100 ns
-0.2
Time
XBL726-3150

Fig. 3

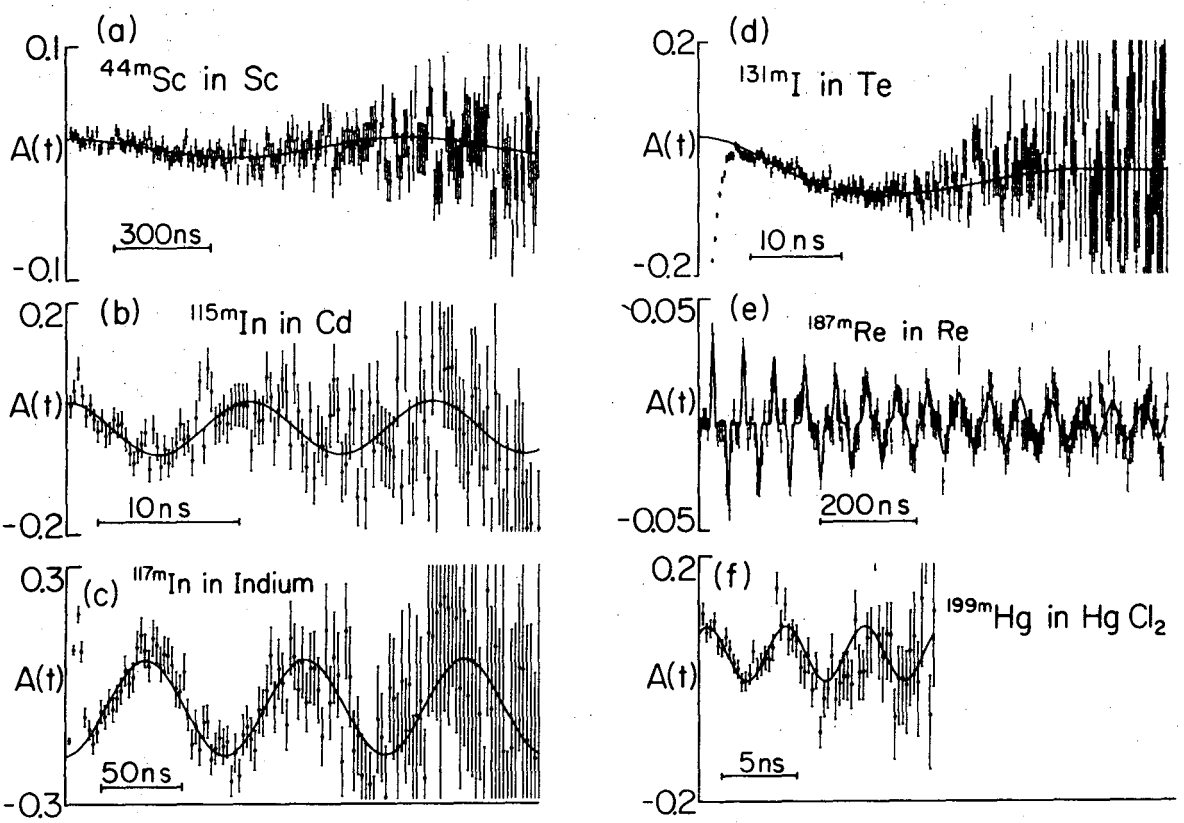
(a)
^{44m}Sc in Sc
0.1
A(t)
-0.1
300ns
(b)
^{115m}In in Cd
0.2
A(t)
-0.2
10ns
(c)
^{117m}In in Indium
0.3
A(t)
-0.3
50ns
(d)
^{131m}I in Te
0.2
A(t)
-0.2
10ns
(e)
^{187m}Re in Re
0.05
A(t)
-0.05
200ns
(f)
^{199m}Hg in Hg Cl$_2$
0.2
A(t)
-0.2
5ns
Time
XBL726-3149

Fig. 4

0 0 0 0 3 8 0 3 0 7 1

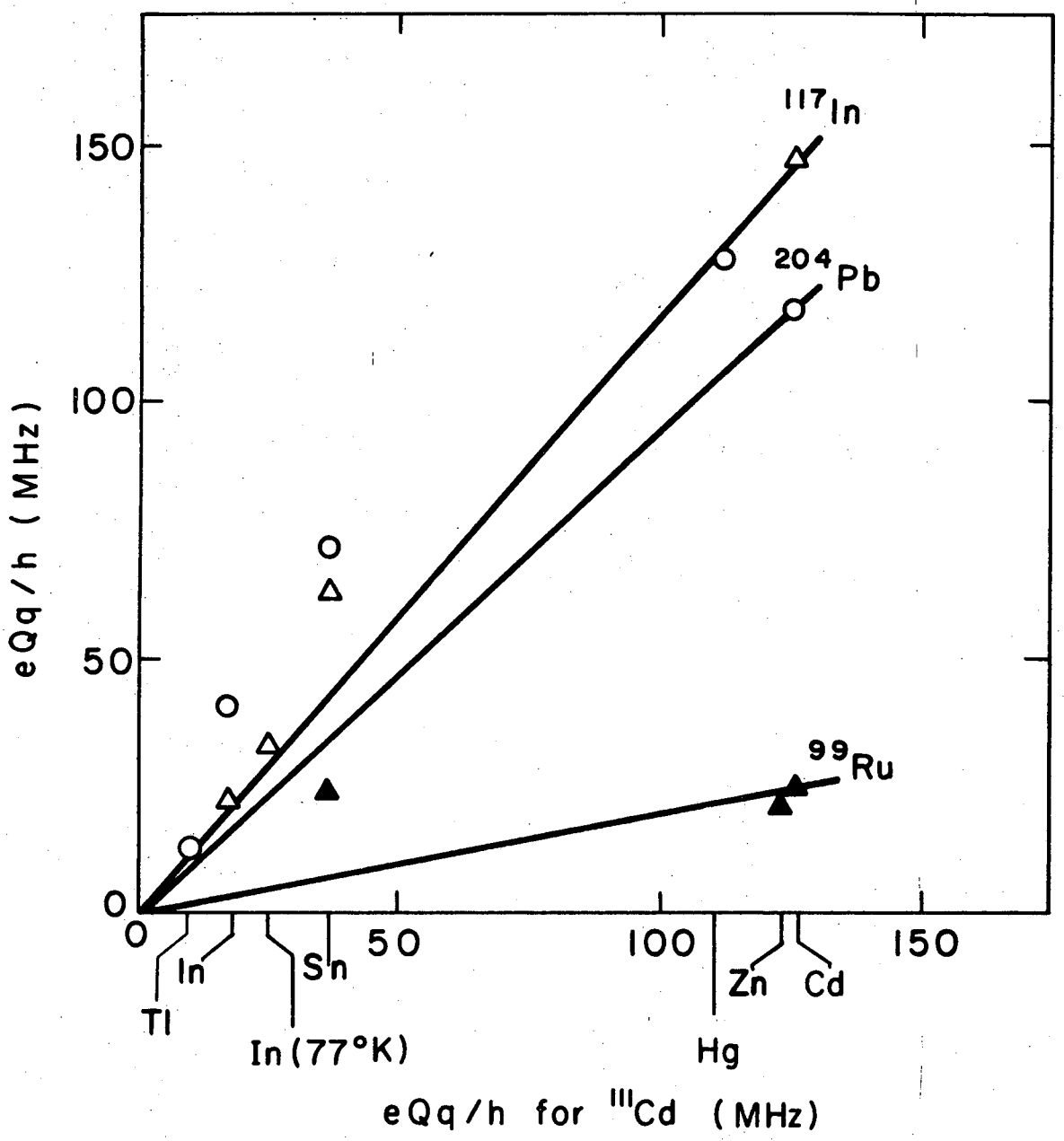

XBL 7210-4223

Fig. 5

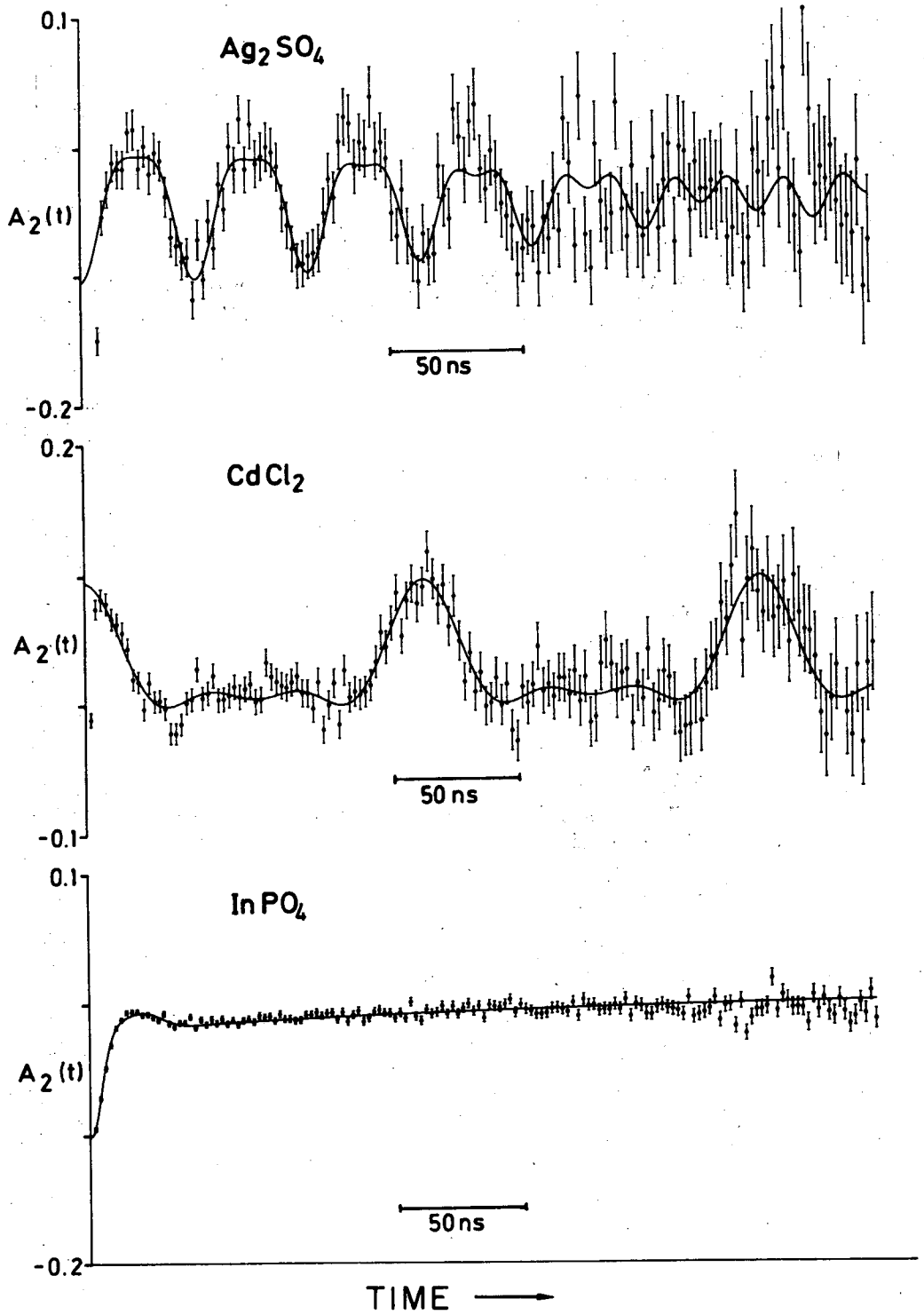
0.1
Ag_2SO_4
$A_2(t)$
50 ns
-0.2
0.2
$CdCl_2$
$A_2(t)$
50 ns
-0.1
0.1
$InPO_4$
$A_2(t)$
50 ns
-0.2
TIME
XBL 724-747

Fig. 6

0 0 0 0 3 8 0 0 3 7 2

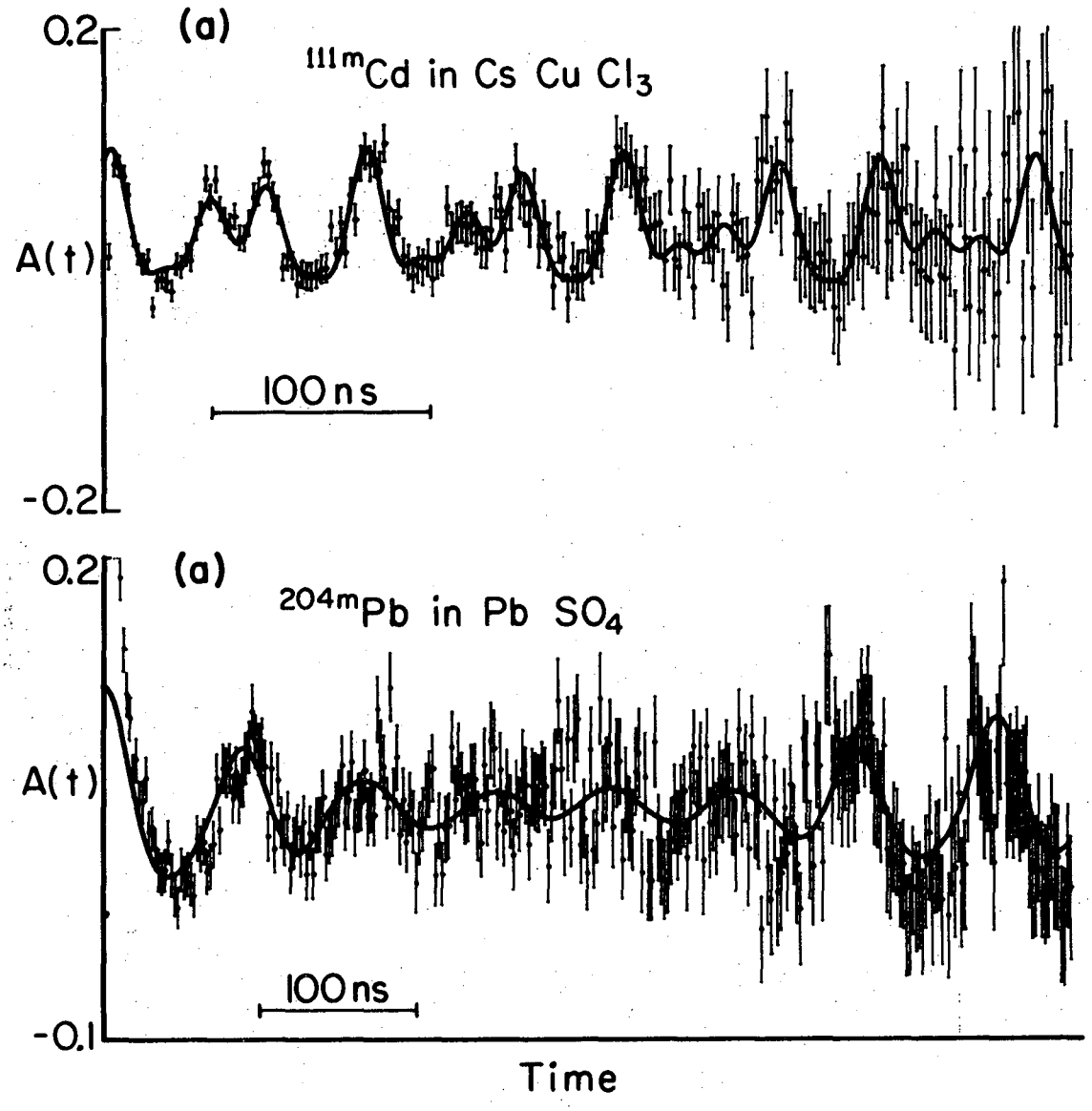

Fig. 7

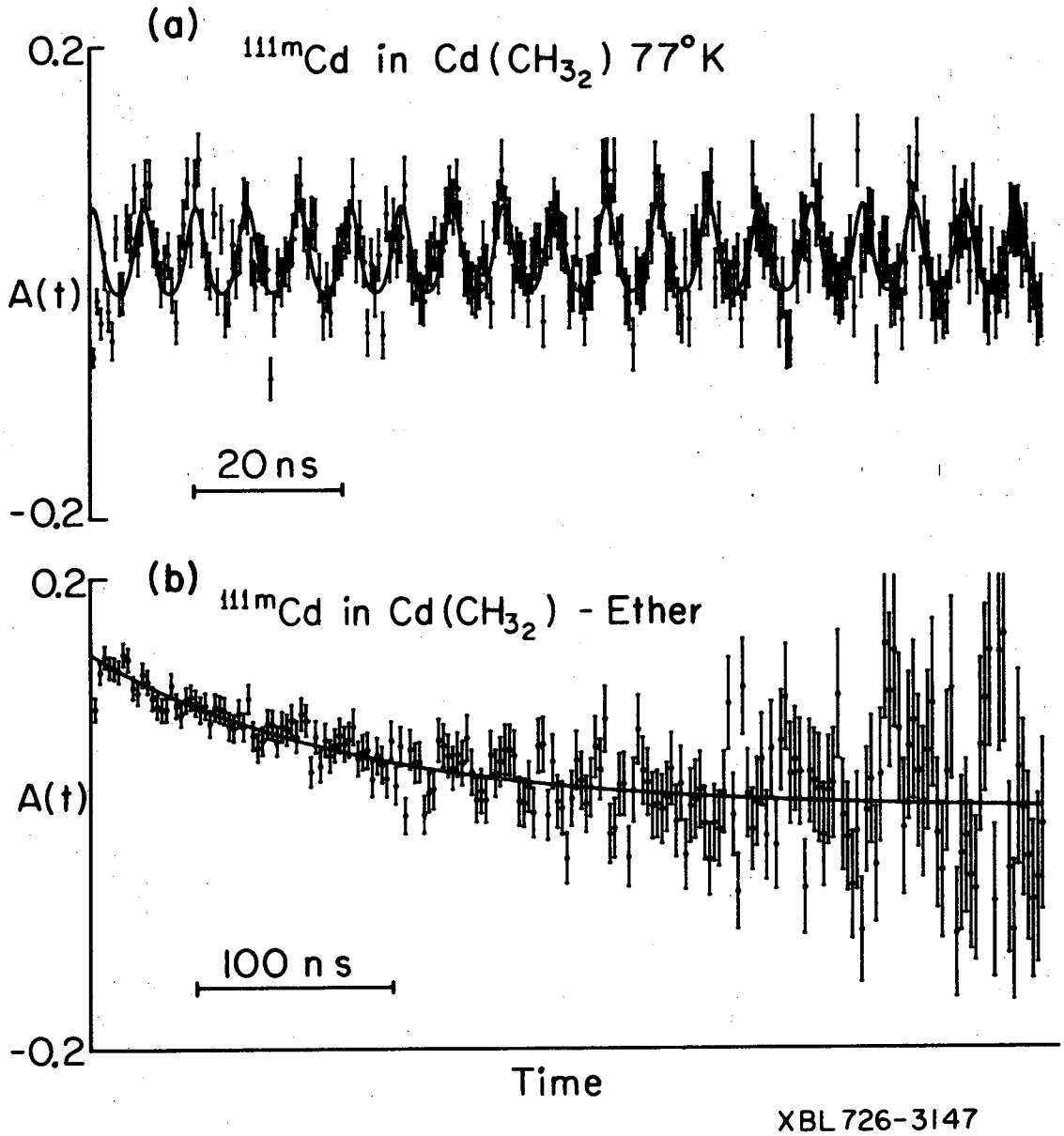
(a)
^{111m}Cd in Cd(CH$_3$)$_2$ 77°K
0.2
A(t)
-0.2
20 ns
(b)
^{111m}Cd in Cd(CH$_3$)$_2$ - Ether
0.2
A(t)
-0.2
100 n s
Time
XBL 726-3147

Fig. 8

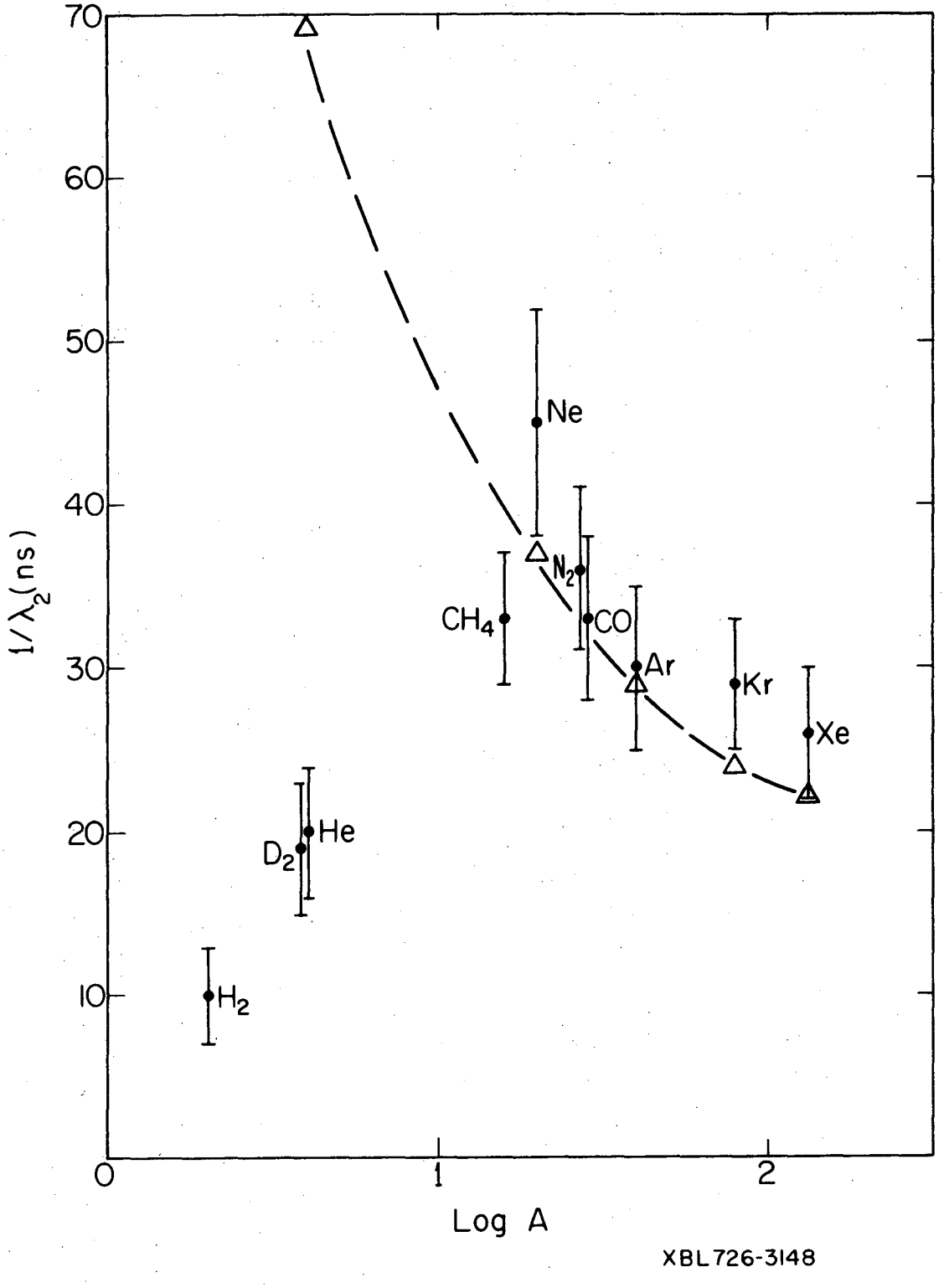
70
60
50
40
30
20
10
0
1
2
$1/\lambda_2$(ns)
Log A
Ne
N_2
CH_4
CO
Ar
Kr
Xe
D_2
He
H_2
XBL726-3148

Fig. 9

LEGAL NOTICE

This report was prepared as an account of work sponsored by the United States Government. Neither the United States nor the United States Atomic Energy Commission, nor any of their employees, nor any of their contractors, subcontractors, or their employees, makes any warranty, express or implied, or assumes any legal liability or responsibility for the accuracy, completeness or usefulness of any information, apparatus, product or process disclosed, or represents that its use would not infringe privately owned rights.

TECHNICAL INFORMATION DIVISION
LAWRENCE BERKELEY LABORATORY
UNIVERSITY OF CALIFORNIA
BERKELEY, CALIFORNIA 94720